Spring 5-13-2023

EFFECT OF GRAPHENE-BASED FILLERS ON THE PROPERTIES OF SUNFLOWER-BASED POLYURETHANE

Vishwa Suthar
Pittsburg State University, vsuthar@gus.pittstate.edu

EFFECT OF GRAPHENE-BASED FILLERS ON THE PROPERTIES OF SUNFLOWER-BASED POLYURETHANE

A Thesis Submitted to the Graduate School
in Partial Fulfilment of the Requirements
For the Degree of
Master of Polymer Chemistry

Vishwa Suthar

Pittsburg State University

Pittsburg, Kansas

May, 2023

EFFECT OF GRAPHENE-BASED FILLERS ON THE PROPERTIES OF SUNFLOWER-BASED POLYURETHANE

Vishwa Suthar

APPROVED:

Thesis Advisor _____
Dr. Ram K. Gupta, Department of Chemistry

Committee Member _____
Dr. Khamis Siam, Department of Chemistry

Committee Member _____
Dr. Timothy Dawsey, National Institute for Materials Advancement

Committee Member _____
Dr. John Franklin, Department of English and Modern Languages

Acknowledgments

Foremost, I would like to express my deepest gratitude to Dr. Ram K. Gupta for being my supervisor, who disclosed many constructive directions for me. His dedication, attentiveness, and critical thinking for the research work are major encouragement to me. He has been a central part of my research and academic course. I would like to recognize Dr. Khamis Siam for being an appreciative and blissful academic advisor. I am grateful to Dr. Timothy Dawsey and Dr. John Franklin for taking a break from their valuable work plan and accepting my invitation to be present on my thesis committee. I would like to acknowledge Dr. Norton, Dr. Peter Dvornic, and Mr. Paul Herring for providing a comprehensive knowledge of polymer chemistry. Thanks should also go to the Chemistry Department of Pittsburg State University and the National Institute for Materials Advancement (NIMA), for delivering scholarships, funding, conference disclosure, and a platform to have valuable experience with several delicate instruments.

I had the pleasure of working with Prashant, Magdalene, Felipe, Sahil, Choi, Tenzin, Prasadi, Udeshika, Himanshu, Teddy, Arjun, Vatsal, Mahesh, Priyesh, Yash, Sagar, Shiva, Wang, and Rishabh. I admire my dad who always trusted and supported my career plans and my mother who always strengthened me with her care and love. I am grateful to my younger brother for being an amusing person and laughing loudly with me. Thanks to my family members for appreciating my achievements which motivates me to do more.

EFFECT OF GRAPHENE-BASED FILLERS ON THE PROPERTIES OF SUNFLOWER-BASED POLYURETHANE

An Abstract of the Thesis by
Vishwa Suthar

The polyurethane market depends greatly on synthetic materials which are environmentally unfriendly. This motivated research to replace petrochemical resources with renewable resources for polyurethane production. Keeping this in mind, this research focused on the use of sunflower oil for the preparation of polyol and its use in polyurethane composition. The reaction mechanism of epoxidation and ring-opening was approached for the conversion of sunflower oil to polyol. During the conversion of sunflower oil, unsaturated groups of sunflower oil were converted into hydroxyl groups of polyol.

Sunflower oil-based polyol was successfully blended with methylene diphenyl diisocyanate (MDI) to form urethane bonds. Confirmative tests such as fourier transform infrared spectroscopy (FTIR), gel permeation chromatography (GPC), viscosity, and hydroxyl number analysis were performed. Very small amounts of graphene-based fillers such as graphene nanoplatelets (GNPs), graphene nanoribbon (GNR), graphene oxide (GO), and reduced graphene oxide (rGO) were separately dispersed into polyol by ultrasonication method to prepare polyurethane composites to enhance the thermal and mechanical strength of the polyurethane. The structure of graphene-based fillers was confirmed by X-ray diffraction study.

Film specimens from polyurethane composites were prepared for mechanical tests such as Shore D hardness, tensile and flexural. In the study of tensile strength, the highest tensile strength recorded was 34.9 MPa for polyurethane/graphene nanoplatelet films

having 0.02 wt.% GNPs. For thermal stability analysis, thermogravimetric analysis (TGA), differential scanning calorimetry (DSC), and dynamic mechanical analysis (DMA) tests were conducted. Almost all polyurethane composite samples were thermally stable up to 280 ^{o}C. The change in thermal stability upon adding graphene-based fillers was analyzed by comparing residual percentages. The surface morphology of the films was studied by water contact angle (WCA), and atomic force microscopy (AFM). The highest WCA was measured at 104.22° for PU with 0.05 wt.% rGO filler. Hence, this research studied the effect of a very small quantity of graphene-based fillers on the sunflower oil-based polyurethane film.

Table of Contents

List of Tables

List of Figures

CHAPTER I

INTRODUCTION

1.1. Polyurethanes

Polyurethane (PU) is a special class of polymers preferred for their facile synthesis routes and applications in different industrial sectors such as automotive, construction, textile insulation, footwear, packaging, automobiles, and bedding, as demonstrated in **Figure 1** [1]. In 1849, Wurtz and Hoffman discovered the urethane or carbamate group by analyzing the reaction between a hydroxylated compound and isocyanate [2]. Afterward, PU was prepared using the reaction of a polyol and diisocyanate by Otto Bayer and his colleagues in Germany, in 1937. Initially, foams, as well as fibers were synthesized. During World War II, some PU coating was employed in the field of aircraft for gloss and for protection of the metal from chemicals and corrosion. In 1954, the industrial manufacturing of foams was initiated [3].

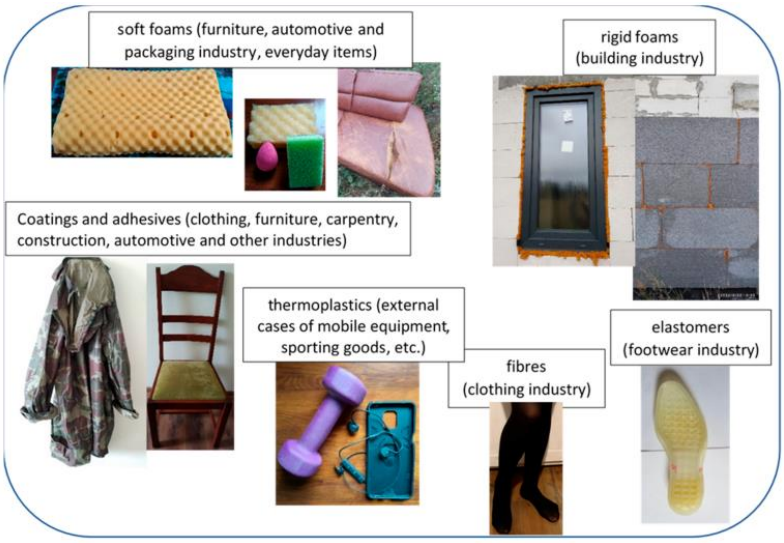

Figure 1. Applications of PUs in different sectors. "Reproduced with permission [3]. Copyright 2021 by the authors. Licensee MDPI, Basel, Switzerland. This article is an open access article distributed under the terms and conditions of the Creative Commons Attribution (CC BY) license (https://creativecommons.org/licenses/by/4.0/)"

PU is distinct from other polymers due to the range of starting materials used. PU has two primary components, a polyol or diol (-OH) and an isocyanate (-NCO). Because isocyanates are highly reactive, the isocyanate's nitrogen atom reacts with the hydrogen atom of the polyol's hydroxyl groups. This results in the urethane linkage also known as carbamate formation between polyol and isocyanate as shown in **Figure 2** [4]. The properties of PU can be manipulated by changing the chemical structures of the isocyanate and/or the polyol. Isocyanates mainly exist in two types - aliphatic and aromatic. Aliphatic isocyanate containing PU is flexible and has a lower glass transition temperature. On the other hand, PU containing aromatic isocyanate have a higher glass transition temperature and is mostly brittle in nature as mentioned in a report [5]. At the same, the type of polyol

also affects the thermal and mechanical properties of the PU. For instance, Ghozali et al. [6] synthesized PU that considered glycerol as a polyol, and caused an increment in thermal property that could be because of higher bond dissociation of formed hydrogen bonding. On the other hand, polyurethane with modified epoxy adopting 1,3-propanediol indicated a reduction in thermal stability, which may be owing to weaker urethane bonding.

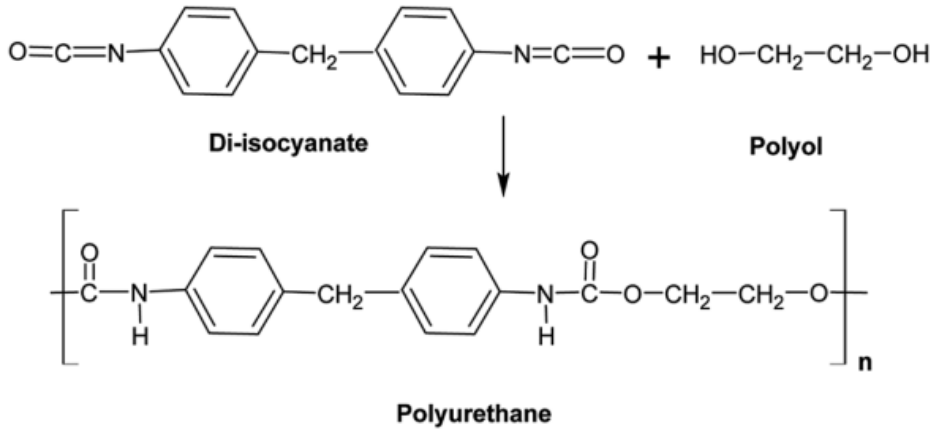

Figure 2. General synthesis route for polyurethane. "Reproduced with permission [4]. Copyright (2016) Royal Society of Chemistry"

Conventionally, both components of PU-polyol [7] and isocyanate [8] are synthesized from petroleum. This results in an enhanced PU in terms of thermal and mechanical properties for commercial production. Different forms of PU such as coating, film, rigid and flexible foam, elastomer, and adhesive are currently manufactured from crude oil particularly. However, crude oil-based PU production has consequences for the environment. Hence, there is a need to find alternative raw materials to replace petroleum in the production of PU.

1.2. Bio-derived polyurethane

Even as crude oil-based PU is highly preferred due to their excellent qualities, scientists are working to determine renewable resources for the PU production. **Figure 3** shows use of bio-based polyurethane products in various applications. Currently, numerous ongoing research for PU fabrication using renewable sources shows attractive properties as commercial PU. The reasons for growing the bio-based PU market are: (1) depleting amount of non-renewable resources such as crude oil affects the price of these resources; and, (2) petroleum products usage also result in carbon emission [9]. These stated impacts of using non-renewable resources provoked the research of renewable sources options for the PU production.

Sustainable sources identified by researchers include vegetable oils [10], vegetable and animal fats [11], starch [12], and soy protein [13]. Using such sustainable resources can be beneficial to the environment by reducing carbon footprints [14]. The current research focuses on the preparation of polyol from sustainable resources using multiple synthesis routes, such as hydroformylation, ozonolysis, epoxidation, ring-opening, and thiol-ene-click. Among mentioned resources, vegetable oils are frequently used raw materials. Vegetable or plant oils, like castor oil, soybean oil, jatropha oil, palm oil, and sunflower oil have been the subject of significant research due to the aromatic ring and the possible hydroxyl group formation which affects the capability of polymer or polyurethane composition [15].

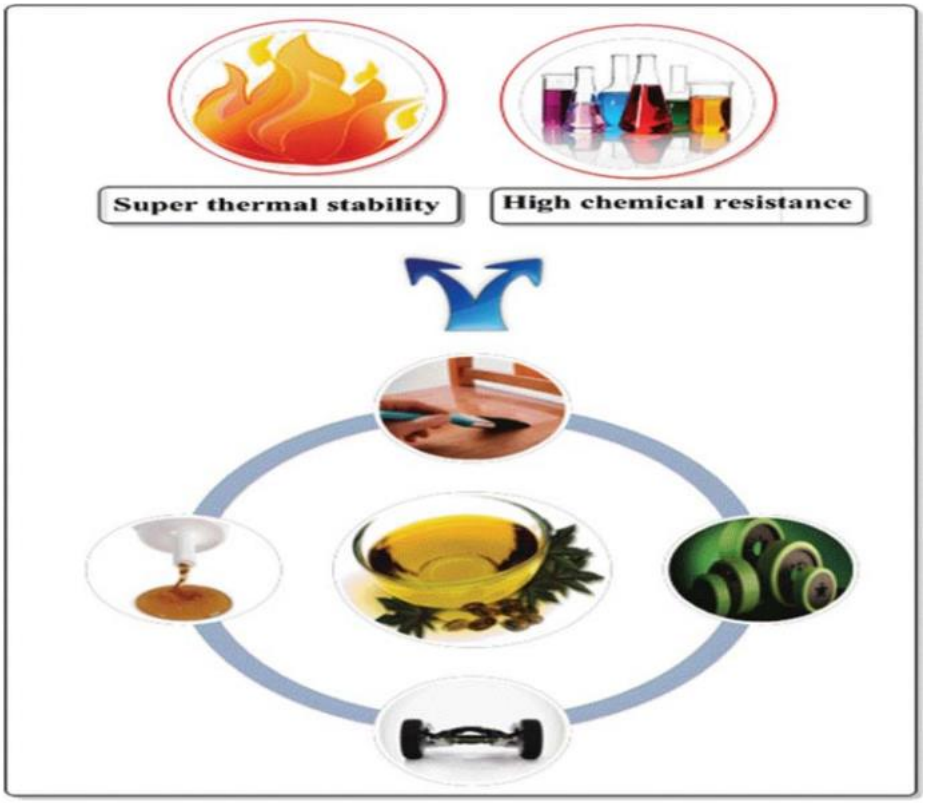

Figure 3. Bio-based polyurethane products in different applications. "Reproduced with permission [16]. Copyright (2018) Taylor & Francis"

A few renewable resources which can be used as a raw material for polyurethane have been investigated by researchers. For example, Mahmood et al. [17] synthesized PU rigid foam from lignin for the application of insulation as well as automobile industries. Moreover, Paraskar et al. [18] developed an air-cured PU coating using three different vegetable oils – linseed oil, karanja oil, and castor oil – for metal coating applications which showed multiple characteristics due to different fatty acid compositions of oils. For adhesive application, a green alga *Entermorpha* that has adhesion property in it, examined by Callow [19].

These sorts of alternatives are possible due to the extensive variety of chemical structures of bio-based sources and many available reactive sides. Moreover, excellent features can be added in different forms of bio-based PUs. In terms of coating, properties such as chemical resistance, superb toughness, and abrasion resistance can be obtained using sustainable sources [20]. Hence, PU matrices carried out from natural resources offered great properties while minimizing environmental impacts. Furthermore, functional groups can be added to the PU structure for additional features. For example, various amine based functional groups were introduced to the PU by Wang et al. [21] for antibacterial property. This type of PU exhibited a variety of functionalities for a list of applications. However, improvements in PUs were required for market assurance.

Besides polyol, experiments are also ongoing for isocyanate made of renewable resources. Bio-derived compounds like carbohydrates, amino acids, lignin based aromatics, and cashew nut shell liquid can be used to develop bio-based isocyanate [22]. Researchers are working on the production of bio-derived isocyanate which combines quality and performance. By doing this, production of PU can be almost 100% biobased.

Furthermore, investigations are also ongoing for PU which can be produced without isocyanate. These are called “non-isocyanate polyurethane” (NIPU). As isocyanates are harmful for human health, it will be beneficial to synthesize the PU without isocyanate while with same properties. The most frequently applied synthesis method for NIPU is carbonation in which cyclocarbonates react with amine for urethane linkage formation. For instance, Javani et al. [23] performed an experiment of soybean oil conversion to carbonated soybean oil and reacted with amine for NIPU preparation.

1.3. Polyurethane composites and applications

Sectors such as aerospace, packaging, and automobile preferred PU as a resin comparative to polyester or other, as PU exhibited toughness [24]. However, along with sustainable ways of PU synthesis, there are specific shortcomings linked with PUs. PU shows performance deficiency because of low thermal stability and mechanical strength. These deficiencies limit many practical utilizations of PU-based products in industries. As a solution, functional groups were added to the PU for supplementary features, and experiments were conducted with additives or fillers additions into the PU matrix. The combination of a filler and the PU solution is known as polyurethane composite (PUC). The fundamental aims of using fillers are upgrading properties and modulating the aspects of the processing path.

Fillers can be classified according to many factors such as the purpose of addition, shape, size, nature, and structure of filler [25]. Fillers can be sorted into two main categories: (1) inorganic which has a subclass of oxides, salts, silicates hydroxides and metals; and (2) organic which has synthetic polymers, natural polymers, carbon, or graphite for organic family. Typically, fillers like kaolin, feldspar, calcium carbonate, talc, and mica are used for the industrial scale. These all showed distinct functions while assembling with any polymer resin or matrix [26]. PUC provides properties like durability, high impact strength, high flexibility, abrasion resistance, low density, and damping ability [27]. For instance, Tawfik et al. [28] synthesized kaolin-based polymer composites and noticed improvement in electrical as well as mechanical strength in the matrix. In another study, thermal stability and mechanical properties were boosted upon blending talcum powder

with PU [29]. Apart from this, some fillers such as aluminium hydroxide $Al(OH)_3$ and, magnesium hydroxide $Mg(OH)_2$ were used as flame retardants when incorporated with PU.

Recently, the invention of graphene based fillers is an essential addition in the field of science and plays a major role in applied science [30] because they have outstanding mechanical, thermal, and optical qualities. Also, graphene is a potent and conductive material [31]. In 2004, Kostya Novoselvo and Andre Geim first detected a single layer of graphene [32]. Multiple synthesis methods standardized its preparation. Out of them, three routes were accessed repeatedly: (1) chemical methods, (2) chemical vapor deposition (CVD) and, (3) mechanical exfoliation from natural graphite.

Various graphene-based materials such as graphene oxide, graphene nanoribbons, graphene quantum dots and carbon nanotubes are available. The applications of graphene materials are numerous as mentioned in **Figure 4**. These distinct forms of graphene are widely in use for producing polymeric composites, sensors, displays, functional inks and the like. In this day and age, graphene is an interesting material for composing electrodes for supercapacitors, secondary batteries, fuel cells, solar cells, and so forth [33].

Figure 4. Properties and application of graphene-based polymer composites.

"Reproduced with permission [34]. Copyright (2017) credit to Versarien"

1.4. Objective of the thesis

The objective of this thesis is to research the use of sunflower oil by converting it to polyol. It was converted to epoxide sunflower oil using the epoxidation method and further sunflower oil-based polyol using a ring-opening mechanism. Iodine value and

epoxy value were determined during conversion of oil to polyol. The polyol synthesis was confirmed by characterization methods such as FT-IR, GPC, hydroxyl value performed prior to the preparation of the PU matrix. Different concentrations of graphene-based fillers were dispersed to the polyol for PU composite fabrication by using ultra sonication. This was followed by graphene dispersed polyol and MDI blended and thermally cured. The synthesized PU composite matrices were studied by standard techniques like TGA, DMA, DSC, WCA, tensile test, flexural test, AFM, and chemical resistance to understand the effect of filler on the properties of PUs.

CHAPTER II

EXPERIMENTAL DETAILS

2.1. Materials

2.1.1. Sunflower oil as a source for polyol

5000 years ago, Native Americans in North America harvested the sunflower also called *Helian annuus L.* Russia, Ukraine, Argentina, and European Union are significant countries that produce sunflowers. At that time, it was used in the food industry. Later, other applications like cosmetics, biofuels, and lubricants were developed for sunflower oil. Sunflower oil mostly contains unsaturated fats (85%) as well as saturated fats (15%) which are desirable for the conversion of polyol [35]. Due to its composition, researchers successfully developed polyol using sunflower oil for polyurethane manufacturing. In the composition of any oil, fatty acids also play a vital role as they define the functional properties of the ultimate PU. Sunflower oil holds 62-69% of linoleic acid and 20-25% of oleic acid [36]. The primary idea of this research starts from the carbon – carbon double bond present in the structure of sunflower oil (**Figure 5**) which modified via epoxidation and ring-opening reactions and ultimately results in attached hydroxyl group [37]. For this experiment, sunflower oil was purchased from a local Walmart of Pittsburg, KS, USA.

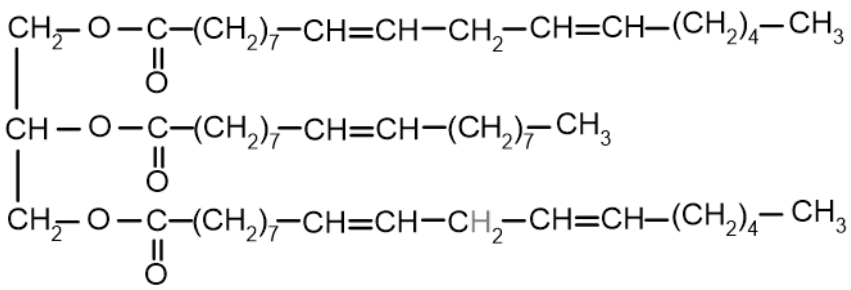

Figure 5. Chemical structure of sunflower oil

2.1.2. Isocyanate

Isocyanate is a highly reactive substance and has a vital role in PU. In the structure of it (**Figure 6**), oxygen has a higher electron density compared to nitrogen and carbon. This brings high reactivity to the functional groups of isocyanates towards nucleophiles. These nucleophiles can be urea, alcohols, amines, water, carboxylic acids, and thiols [38]. There are several types of isocyanates used for the synthesis of PU, such as toluene diisocyanate (TDI), and hexamethylene diisocyanate (HDI) [39]. Here, Rubinate M isocyanate also named as methylene diphenyl diisocyanate (MDI) was gifted from Huntsman (The woodlands, TX, USA).

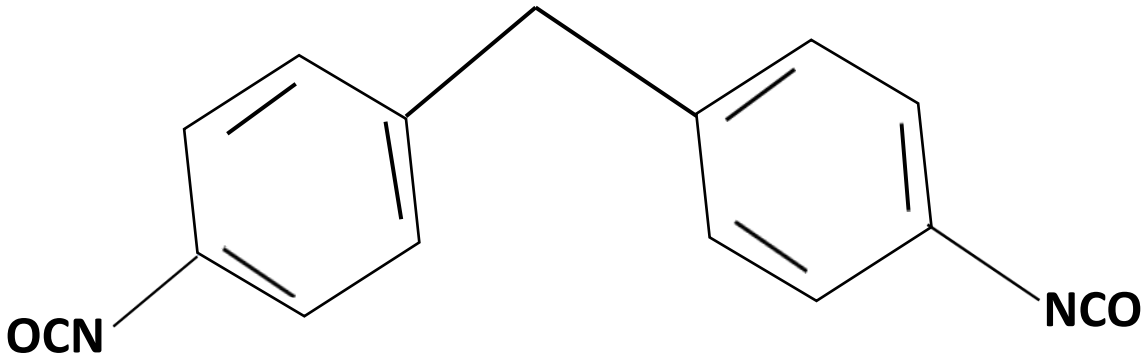

Figure 6. Chemical structure of methylene diphenyl diisocyanate.

2.1.3. Graphene-based fillers

Graphene is a promising material as a filler and plays a vital role in the growth of next-generation polymer composites. Graphene can be treated further via different synthesis routes to functionalize its structure. Four distinct types of modified graphene-based compounds such as graphene nanoplatelets (GNPs), graphene nanoribbons (GNR), reduced graphene oxide (rGO), and graphene oxide (GO) were utilized as fillers.

2.1.3.1. Graphene nanoplatelets

GNP is platelet-like structure as shown in **Figure 7**. Several factors like lateral size of the flakes, defect concentrations, thickness, and aspect ratio depend on the methods of its preparation. There are various methods used to obtain GNP powder such as shear exfoliation, the exposure of acid-intercalated graphite to microwave radiation, ball-milling and so forth. However, GNP is generally acquired by the liquid phase exfoliation method as reported by P. Cataldi [40]. GNPs have desirable qualities such as tensile strength, fracture toughness, and low density. Moreover, it has good load transferability from polymer to filler for the reinforcement application, although, the reinforcement application is limited by agglomeration owing to its sheet stacking. For this research, GNPs were bought from Sigma Aldrich, USA.

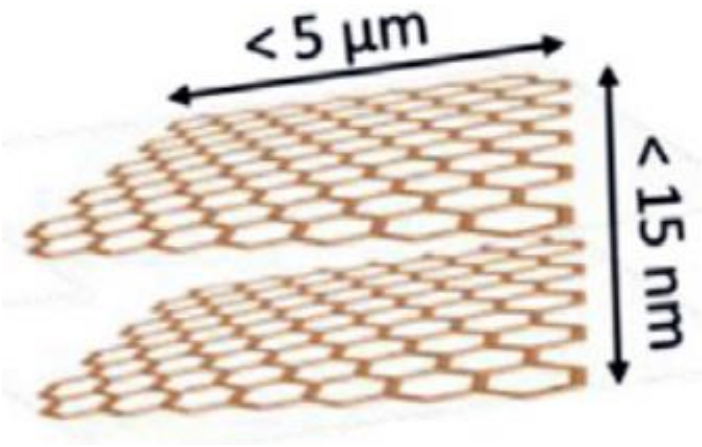

Figure 7. Chemical structure of graphene nanoplatelets. "Reproduced with permission [41]. Copyright (2017) Elsevier"

2.1.3.2. Graphene nanoribbon

As its name suggests and as shown in **Figure 8**, GNR is a ribbon-like form of sp^2 carbon atoms, composed of quasi-1D structured along with a narrow width of < 10 nm. These can be fabricated with various methods like chemical vapor deposition, plasma etching route, and lithography. GNRs have excellent mechanical, thermal, electrical, and optical properties. GNRs are employed in the fabrication of electrodes, supercapacitors and sensors, drug delivery, polymer composites, and are used in catalytic reactions [42], [43]. In this research, GNRs were fabricated by chemically unzipping multi-walled carbon nanotubes (MWCNTs). MWCNTs was purchased from Sigma Aldrich, USA.

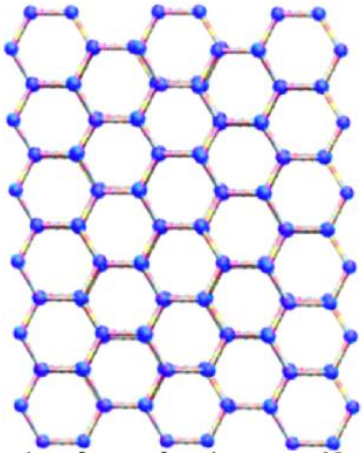

Figure 8. Chemical structure of graphene nanoribbon. “Reproduced with permission. [44] Copyright (2019) Springer”

2.1.3.3. Reduced graphene oxide

Reduced graphene oxide is the reduced form of graphene oxide and is closer to pristine graphene in terms of properties. This leads to a reduction in the number of oxygen groups in the compound (**Figure 9**). rGO can be prepared by various reduction methods of GO, including chemical, thermal, and photothermal reduction. Based on these methods, the reduction degree will be varied, and this range of reduction degree leads to property alterations. This change in terms of chemical structure also enhances the properties of rGO, like mechanical strength, and dispersibility of filler. rGO is used in the field of manufacturing sensors, supercapacitors, batteries, polymer composites, and membranes [45], [46]. For this experiment, rGO was purchased from ACS Materials, USA.

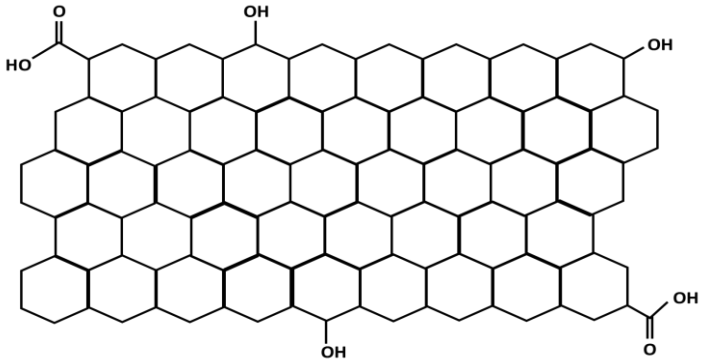

Figure 9. Chemical structure of reduced graphene oxide.

2.1.3.4. Graphene oxide

Currently, GO is emerging as an interesting material for various applications. In 1859, Benjamin Brody synthesized the first GO [47]. GO can be obtained by the oxidation of graphene. The most common method is the Hummers - Offeman method to produce GO [48]. The structure of GO, as shown in **Figure 10**, has a hexagonal carbon structure, along with carbonyl (C=O), hydroxyl (-OH), alkoxy (C-O-C), carboxylic acid (-COOH), and several oxygen groups. These functional groups induce the potential of surface functionalization along with higher solubility [46]. The potential applications of GO are sensors, drug-delivery systems, polymer composites, and energy storage devices [49]. For this experiment, GO was purchased from Sigma Aldrich, USA.

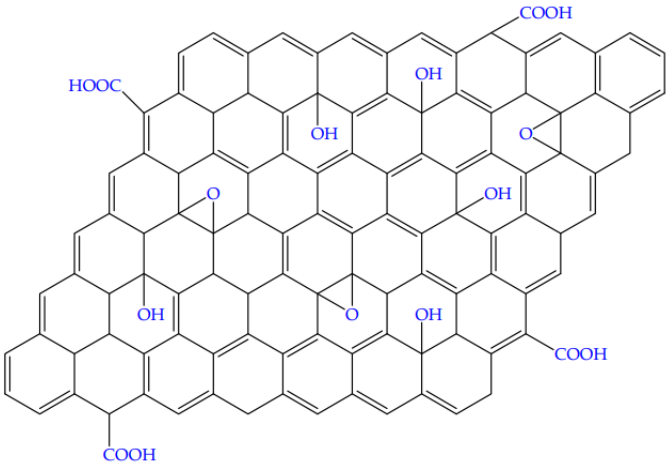

Figure 10. Chemical structure of graphene oxide. "Reproduced with permission [50]. Copyright 2021 by the authors. Licensee MDPI, Basel, Switzerland. This article is an open access article distributed under the terms and conditions of the Creative Commons Attribution (CC BY) license (http://creativecommons.org/licenses/by/4.0/)."

2.2. Synthesis of polyol from sunflower oil

For the conversion of polyol from sunflower oil, epoxidation followed by ring-opening reaction method was followed.

2.2.1. Epoxidation of sunflower oil

As shown in **Figure 11**, hydrogen peroxide and acetic acid act as oxygen donors and oxygen carriers, respectively. Consequent to the reaction of these two, peracetic acid is formed. This peracetic acid further breaks down the double bond existent in the sunflower oil and transforms it into the epoxy rings. Here, the conversion of double bonds to the epoxy rings is performed under acidic conditions as well as temperatures of 5 to 70 °C.

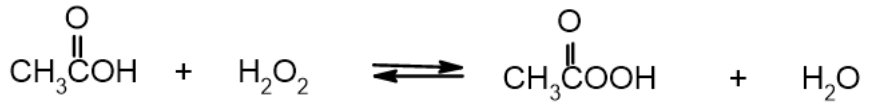

Figure 11. Formation of peracetic acid

In this route, a molar ratio of 1:0.5:1.5 was followed for double bond/ acetic acid/ hydrogen peroxide. 300 g of sunflower oil, 150 ml of toluene and 75 g of Amberlite resin (catalyst) were mixed in a three-necked round bottom flask. With a modulating temperature system, the flask was placed in a water bath. The temperature was decreased to 5 °C while the mixture was continuously stirred. 43.9 ml of acetic acid was added, followed by 180 ml of hydrogen peroxide (30%). Both compounds were added in a dropwise manner to avoid possible superheating from the exothermic epoxidation process [51]. The solution was stirred for 7 hours at 70 °C. The solution then underwent a filtration process after being cooled to ambient temperature.

The purification of the solution was accomplished by washing with 10% brine in a separatory funnel. To eliminate the aqueous layer from the oil, brine was added by intervals, and was shaken vigorously. Anhydrous sodium sulfate was mixed as a drying agent and agitated with the solution. Next, sodium sulfate was strained followed by rotary evaporation at both high and low vacuum to remove the leftover solvents from the solution. The epoxidation process of sunflower oil was confirmed by epoxy value determination, FT-IR, and GPC tests. The yield for ESFO was around 87%.

2.2.2. Polyol from epoxide sunflower oil by ring-opening method

An epoxy ring is basically made up of an oxygen attached to two adjacent carbons. During the ring-opening reaction, a nucleophilic attack by a beta-substituted hydroxyl group was enabled due to the existence of electrophile oxygen of the epoxy ring. Diols, carboxylic acid, and mono alcohols are the most exposed nucleophiles for ring-opening [52], [53].

In this synthesis, tetrafluroboric acid (HBF_4) was used as a catalyst. To execute the ring-opening reaction, methanol was added to a three-neck round flask in a 7:1 molar ratio to the epoxy group at 65 to 70 °C. The flask was also fitted with a condenser and dropping funnel. Following that, 0.585 g of tetrafluoroboric acid (equal to 48 wt.% of water and 0.05 wt.% of methanol and ESFO) was added to the mixture. ESFO was introduced into the solution using a dropping funnel and was stirred for 70 minutes with an attached condenser. After the addition of the ESFO, the solution was refluxed for 1 hour in the presence of a condenser to avoid methanol evaporation. When the reaction was cooled, Lewitt MP 64 ion exchange resin was added to the flask and agitated for 30 minutes to neutralize the system. The resin was strained followed by pH determination of the mixture. After verifying a neutral pH, rotary evaporation of high and low vacuum was conducted for more than 2 hours. The yield for the conversion of ESFO to SFO polyol was 80.5%. The final polyol was characterized by standard techniques including hydroxyl value determination and viscosity. An illustration of epoxidation followed by ring-opening reaction is shown in **Figure 12**.

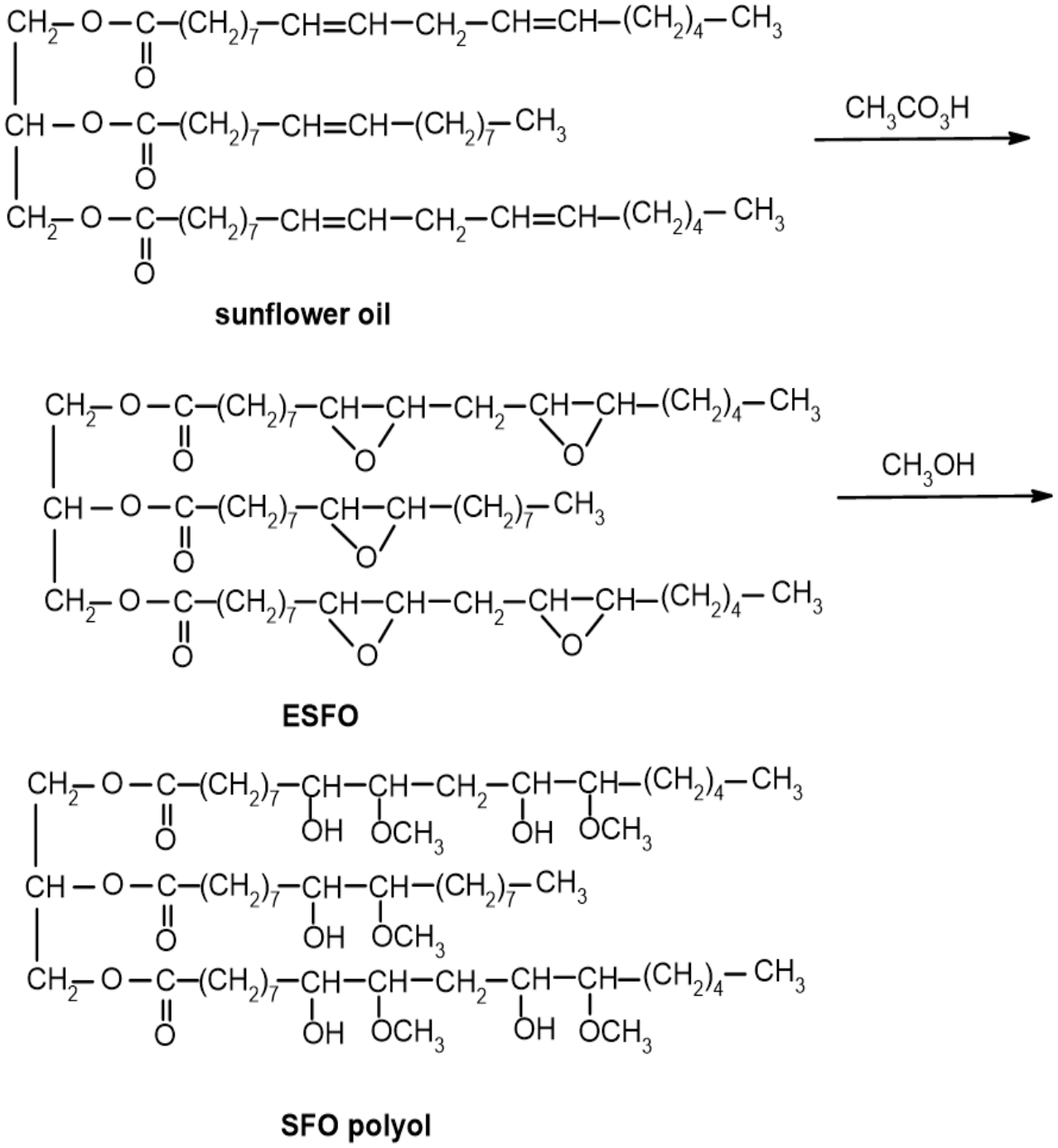

Figure 12. Synthesis route of polyol from sunflower oil by epoxidation and ring-opening method

2.3. Characterizations of sunflower oil-based polyol

2.3.1. Iodine value

Iodine value indicates the number of double bonds that exist as an unsaturated material, depending on the amount of iodine value that will react with 100 g of the tested sample. The *Hanuš* method (IUPAC 2.205) was used for this confirmative test, which determined the amount of double bonds that exist in the sunflower oil. 0.2 g of sunflower oil was dissolved in 10 ml chloroform ($CHCl_3$) solvent in an Erlenmeyer flask. Then, 20 ml of Hanus reagent – iodine monobromide (IBr) was poured into the mixture. The flask was slightly shaken followed by leaving it in the absence of light for 1 hour. Next, 20 ml of 10% potassium iodide (KI) solution and 50 ml of HPLC grade water were poured into the flask and stirred for uniformity. Starch indicator (6 drops) was added to the mixture, resulting in a blue mixture. The mixture was titrated using sodium thiosulphate ($Na_2S_2O_3$) until a colorless mixture was formed. The iodine value was finalized by an average of 3 differently recorded values.

2.3.2. Epoxy value

The determination of epoxy oxygen content (EOC%) was used to examine and confirm the formation of epoxide group from double bond. The value was determined by following the ACS PER-OXI method [54]. Tetraethylammonium bromide (TEAB) and glacial acetic acid were used for this test. In 50 ml of TEAB solution, 0.5 g of epoxide sunflower oil was dissolved. As an indicator, 1 drop of crystal violet was added to the mixture followed by titration with 0.1N perchloric acid ($HClO_4$). The endpoint of the titration was indicated by a change in color from blue to green. The difference in $HClO_4$

volume was used in the calculation of EOC% of epoxide sunflower oil. The test was performed 3 times; the average value was the final EOC%.

2.3.3. Hydroxyl value

The hydroxyl value or OH number was determined by test method phthalic anhydride pyridine (PAP) by following IUPAC 2.241. For that, 0.5 g of SFO polyol was dissolved in 10 ml of a hydroxyl solution (polyol) in a glass bottle. The bottle was capped and placed in an oven for 70 minutes at 100 °C. The bottle was shaken in intervals of 15 minutes. Then, the solution was left outside of the oven and cooled to room temperature. After the solution cooled, 20 ml of isopropanol and 10 ml of HPLC-grade water were added and agitated for 10 minutes. The solution was titrated using 1 N sodium hydroxide (NaOH) until it turned pink. The difference in NaOH volume was used for the calculation of hydroxyl value. Three samples were tested; average value was accounted as a hydroxyl number.

2.3.4. Fourier-transform infrared spectroscopy

Fourier-transform infrared spectroscopy (FT-IR) method was used to obtain the spectra for synthesized materials at room temperature. The PerkinElmer Spectrum Two Spectrophotometer was operated to obtain the individual spectrum displayed for studied materials (**Figure 13**). FT-IR is a quick approach to recognize the present functional groups in a material. Moreover, solvents are usually not required to perform this test.

Figure 13. FT-IR spectrometer

2.3.5. Gel permeation chromatography

Gel permeation chromatography is often used as an analysis technique for polymers, which is one type of size-exclusion chromatography. This technique separates components based on their molecular weight. Here, a GPC instrument by Waters (Milford, MA, USA) was used to confirm the synthesis of polyol from sunflower oil. Polyol, epoxide oil, and sunflower oil were tested as a function of molecular weight (**Figure 14**). The GPC arrangement consisted of four 300 × 7.8 mm phenol gel 5 μm columns. These columns have pore sizes of 50, 102, 103, and 104 $A°$. Tetrahydrofuran (THF) was used as an eluent with 1 ml/min flow rate at 30 ^{o}C.

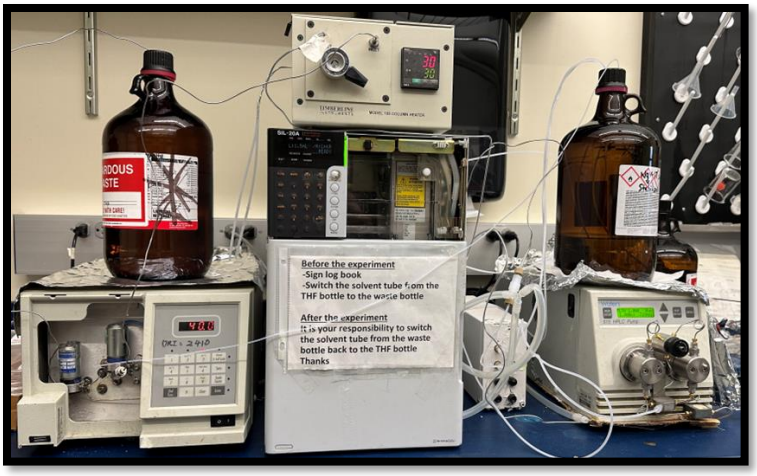

Figure 14. Instrumental setup of GPC

2.3.6. Viscosity

The viscosity of polyol, epoxide oil, and sunflower oil was determined by an AR 2000 dynamic stress rheometer by TA Instruments, USA (**Figure 15**). The rheometer was facilitated with a cone plate which has 25 mm of cone diameter and 2^{o} of angle. The temperature while determining the viscosity was 25 ^{o}C with a linearly increasing shear stress from 1 to 2000 Pa. Viscosity is an essential parameter to determine the flow resistance of the material. A high viscosity indicates a high molecular weight whereas, a low viscosity indicates a low molecular weight of material. Moreover, low viscosity corresponds to a facile processing of the material.

Figure 15. AR 2000 dynamic stress rheometer

2.4. Synthesis of graphene nanoribbons

The unzipping method of multi-walled carbon nanotubes was used for the synthesis of GNRs filler. As illustrated in **Figure 16**, 1 g of MWCNTs were mixed with 280 ml of concentrated sulfuric acid (H_2SO_4) and 32 ml of concentrated phosphoric acid (H_3PO_4); dispersed using a magnetic stirrer. With constant stirring, 10 g of potassium permanganate ($KMnO_4$) was slowly added to the mixture at 65 ^oC. For the next 4 hours, the mixture was left in the same condition. After that, the mixture was cooled to 25 ^oC followed by pouring above 800 ml of iced water and 40 ml of hydrogen peroxide (30% H_2O_2) solution. Next, the mixture was washed in succession with hydrochloric acid (30%), and ethanol (100%). The obtained compound was dried in a vacuum at 65 ^oC. The final black colored powder – GNRs is further used as a filler in PU.

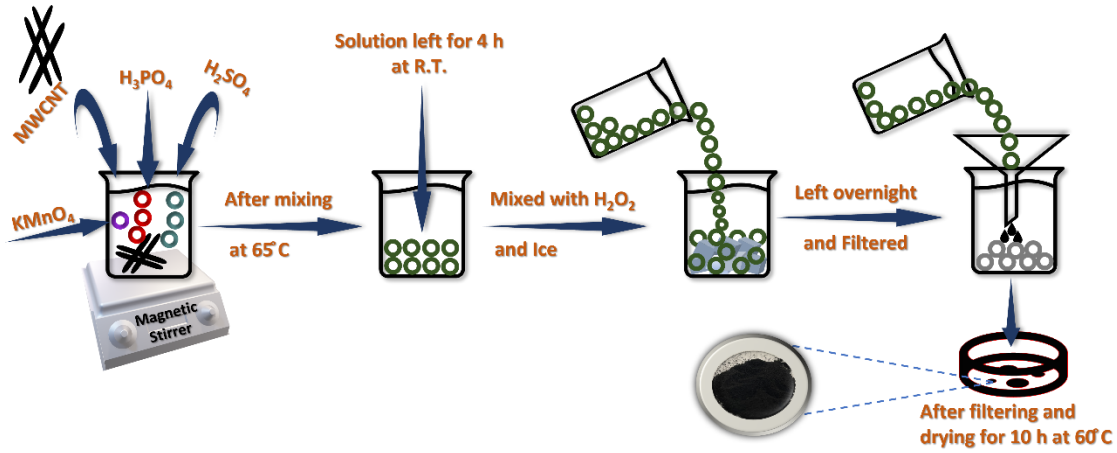

Figure 16. Schematic illustration of graphene nanoribbon preparation

2.5. Characterization of reinforcement materials

2.5.1. X-ray diffraction

The XRD of four fillers: GNP, GNR, rGO, and GO were studied by X-ray diffractometer to obtain an atomic level information like spacing between planes in the structure. Copper ($Cu_{\propto}$) = 1.5406 $A°$ was used as a source to generate X-rays at an applied voltage of 40 kV. The X-ray beams were bombarding the structure are then diffracted in different directions. XRD-6000 from Shimadzu was used to understand the structure of fillers as shown in **Figure 17**.

Figure 17. X-ray diffractometer

2.6. Formulation of bio-based PU composite

For efficient dispersion of fillers, the mixture of polyol and a graphene-based filler was mixed using a bath sonicator for two hours. Three different concentrations 0.01, 0.02, and 0.05 wt.% of filler were dispersed in polyol. After dispersion, filler dispersed polyol was blended with an isocyanate in a molar ratio of 1:1. The solution was poured into the Teflon petri dish and cured in an oven at 70 °C for 90 minutes. The illustration of PUC formulation was shown in **Figure 18**. The rectangular stripes of 10 mm length and 1 mm width were prepared from the synthesized matrix for further characterization. The composition of each component is mentioned in **Table 1**. Digital pictures of PUC are shown in **Figure 19**.

Table 1. Composition of PUC matrix

Sample code	GNP (wt. %)	GNR (wt. %)	rGO (wt. %)	GO (wt. %)	SFO polyol (g)	Isocyanate (g)
Neat	-	-	-	-	14	6.5
GNP1	0.01	-	-	-	14	6.5
GNP2	0.02	-	-	-	14	6.5
GNP3	0.05	-	-	-	14	6.5
GNR1	-	0.01	-	-	14	6.5
GNR2	-	0.02	-	-	14	6.5
GNR3	-	0.05	-	-	14	6.5
rGO1	-	-	0.01	-	14	6.5
rGO2	-	-	0.02	-	14	6.5
rGO3	-	-	0.05	-	14	6.5
GO1	-	-	-	0.01	14	6.5
GO2	-	-	-	0.02	14	6.5
GO3	-	-	-	0.05	14	6.5

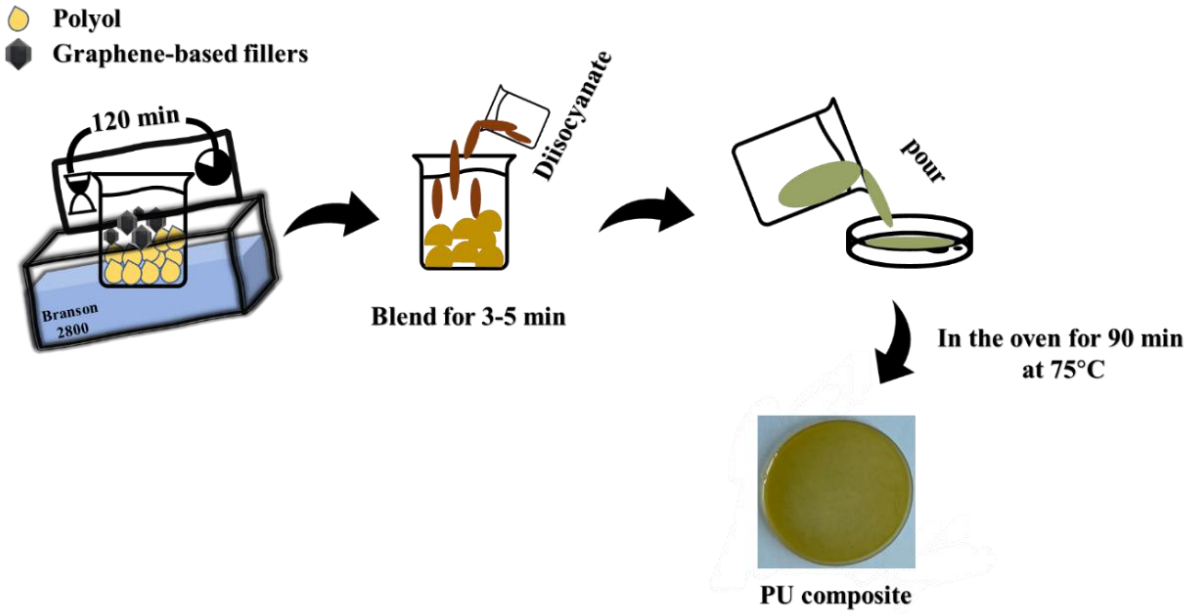

Figure 18. Schematic diagram of polyurethane formulation route

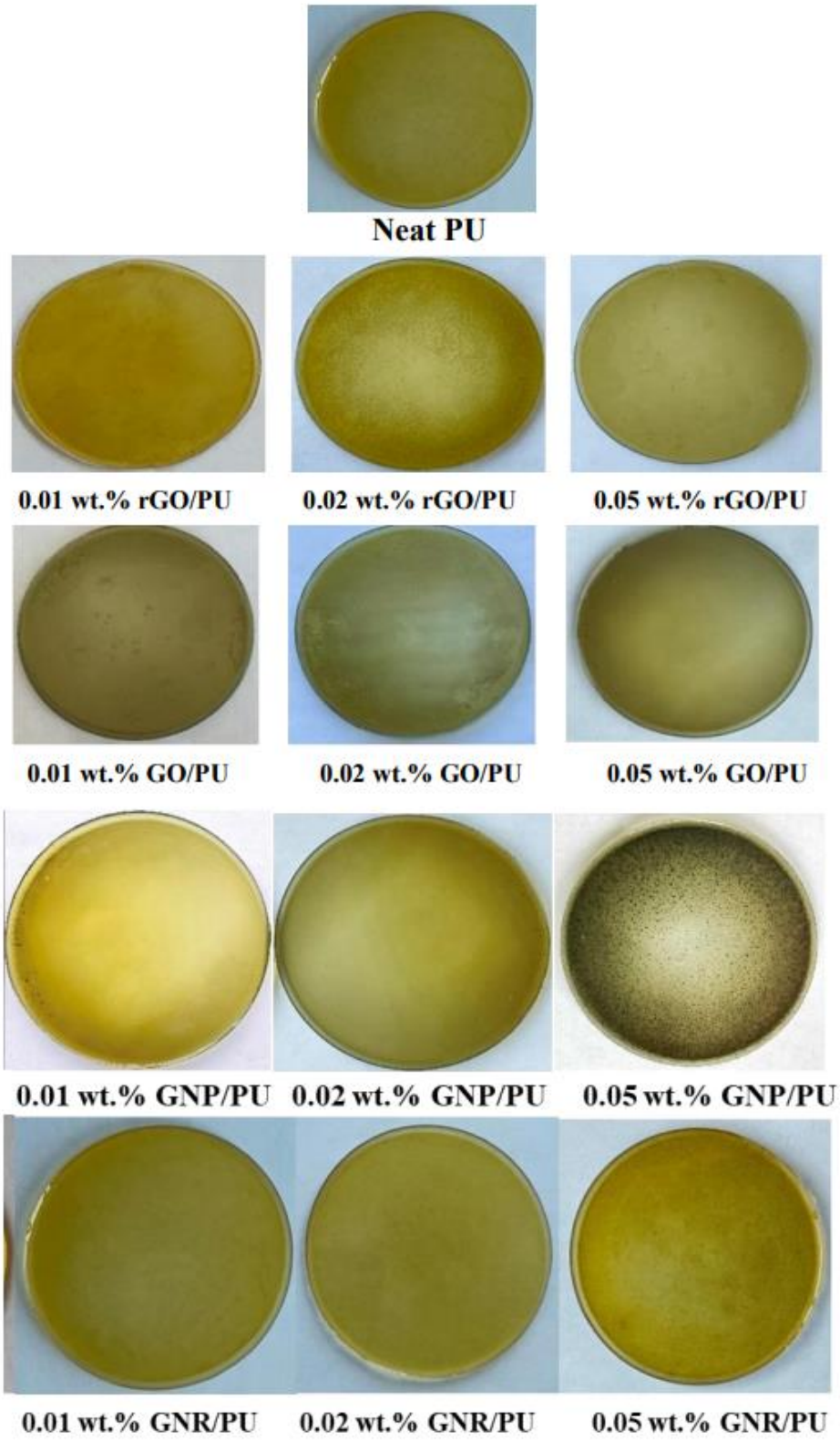

Figure 19. Digital pictures of PUC samples

2.7. Characterizations of the bio-based PU matrix

2.7.1. Thermogravimetric analysis

Basically, thermogravimetric analysis is an analysis of the mass of material that is observed over time with change in temperature. The analysis of mass changes offers details about thermal decomposition, phase transition, solid-gas reactions (oxidation or reduction), and absorption. Here, TGA analysis was conducted using analyzer TGA Q550 by TA Instrument (**Figure 20**). The test was performed for PU composite samples using temperature range of 25-700 ^{o}C, while the ramp rate was 10 ^{o}C/min. This test was completed under nitrogen atmosphere. Moreover, the residual percentage of the samples was compared for thermal stability.

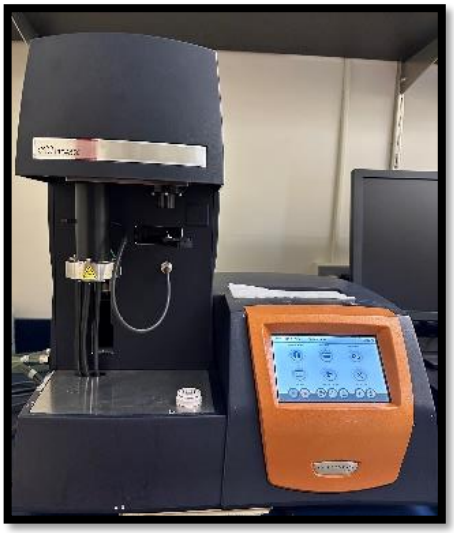

Figure 20. Thermogravimetric analyzer

2.7.2. Differential scanning calorimetry

Differential scanning calorimetry (DSC) is a technique to measure the difference in the heat capacity needed to increase the temperature of a sample as a function of temperature. For polymeric materials, DSC is usually used to examine their thermal transitions-glass transition temperature (Tg), melting temperature (Tm), and crystallization temperature (Tc). Here, a differential scanning calorimeter DSC Q100 by TA Instrument was used with an attached refrigerated cooling system (**Figure 21**). This model of calorimeter has the design of a single furnace, and it measures the difference of heat flux between the sample and a reference. The sample was prepared using a Hermetic pan and lid. The temperature range used for testing was -50 to 260 ^{o}C while the ramp rate was 10 ^{o}C/min.

Figure 21. Differential scanning calorimeter

2.7.3. Dynamic mechanical analysis

Dynamic mechanical analysis (DMA) is a useful technique to study the viscoelastic behavior of polymers. In this technique, stress is applied while measuring the strain of the sample. Moreover, the storage modulus is determined by observing applied variations in the temperature and frequency of the stress. This approach can be useful to recognize transitions and Tg of the material. Here, DMA was conducted by dynamic mechanical analyzer DMA Q800 by TA Instrument (**Figure 22**). The clamp "tension film" was selected for DMA testing. The films were prepared 5-30 mm long, 6.5 mm wide, and 2 mm thick. The temperature range of 30-150 ^{o}C and ramp rate was 3 ^{o}C/min during the testing. The storage modulus and loss factor (tan δ) was determined for the samples.

Figure 22. Dynamic mechanical analyzer

2.7.4. Tensile strength

Tensile strength can be defined as the required stress to stretch the sample before it breaks down. Tensile strength majorly depends on environmental conditions and defects on the sample's surface. In this experiment, the tensile strength of films was determined using a universal tester by Instron 3367 with Blue Hill software (**Figure 23**). ASTM D638 method was followed for this testing. The sample was prepared of 80 mm length, 10 mm width, and 2 mm thickness. The sample was pulled by a tensometer using a crosshead speed of 2 mm/min. The temperature was 25 ^{o}C for both environment and sample. The highest point of tensile stress-strain was evaluated as tensile strength and mentioned with unit megapascals (MPa). By considering the required higher force, the optimum sample was determined. This suggests a specific amount of force or tension can be allowed by the sample before fracturing. For accuracy, 3 samples of each type of PUC were tested and an average of that was noted.

Figure 23. Universal testing machine

2.7.5. Three-point flexural test

A three-point flexural test can be used to determine flexural strain-stress of the sample. This test evaluates the required force to bend a beam-like sample. Here, a three-point bending machine MTS Q-test by Sintech (**Figure 24**) and TestWorks QT software was used to determine the flexural strength of films. The crosshead was proceeded with 2 mm/min speed until the fracture of the sample. The temperature was 25 ℃ at the time of testing. The ASTM D790 method was followed in this test. 2 mm thick and 10 mm wide specimens were prepared for this testing.

Figure 24. Three-point flexural testing machine

2.7.6. Hardness

Hardness of the material suggests a resistance to indentation. The hard material shows higher scale, whereas the soft material shows lower scale for hardness. Typically, polymeric material's hardness is measured. Here, a Shore D durometer by PTC Instrument (**Figure 25**) was used to obtain the indentation hardness of films. This durometer scaled the depth of an indentation in a material originated due to applied force on a indentor. The temperature was 25 ^{o}C while measuring the hardness. ASTM D2240 was followed for the shore D hardness measurements of films.

Figure 25. Shore D durometer

2.7.7. Water contact angle

The water contact angle (WCA) evaluates the wettability of the material by measuring the angle of liquid-solid surface interface. This angle also corresponds to the roughness of the sample's surface. The high roughness of the surface results in higher WCA and low roughness results in lower WCA. For a solid surface, WCA $< 90^{o}$ indicates hydrophilic surface, whereas WCA $> 90^{o}$ indicates hydrophobic surface. In this experiment, the WCA was measured by Goniometer by Ossila which has an optical system (**Figure 26**). The WCA of a film's surface was analyzed by a high-resolution camera located in goniometer with Ossila software. All measurements were performed at room temperature.

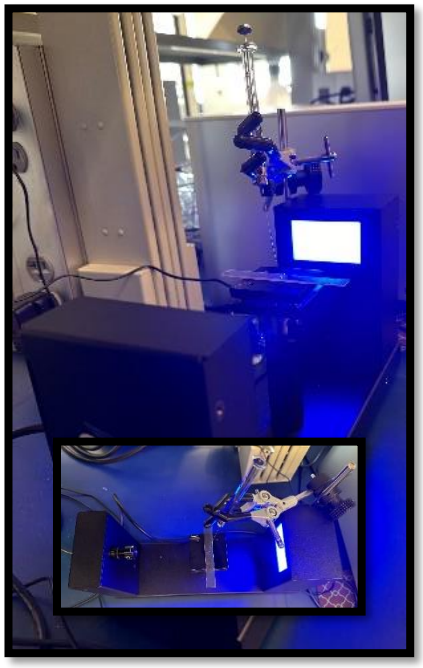

Figure 26. Contact angle goniometer

2.7.8. Atomic force microscopy

In AFM, a probe is scanned over a surface and the motion of the cantilever with a probe is monitored to create a 3D image of the surface. A cantilever is made up of silicon or silicon nitride. It has a nanometer level of resolution probe, which can provide data of manipulation, force measurement, and topographic imaging. Particularly in imaging, the probe's reaction to the force imposed by a sample can draw up the topography image (three-dimensional) of the surface. AFM can be conducted in three different modes as a function of a tip's movement, contact mode, tapping mode, and non-contact mode. The tapping mode is often operated because it avoids the tip adhering issues to the surface. In this experiment, a high resolution - atomic force microscope by AFM workshop was

operated for the surface morphology study of films. The AFM images were prepared using Gwyddion software (**Figure 27**).

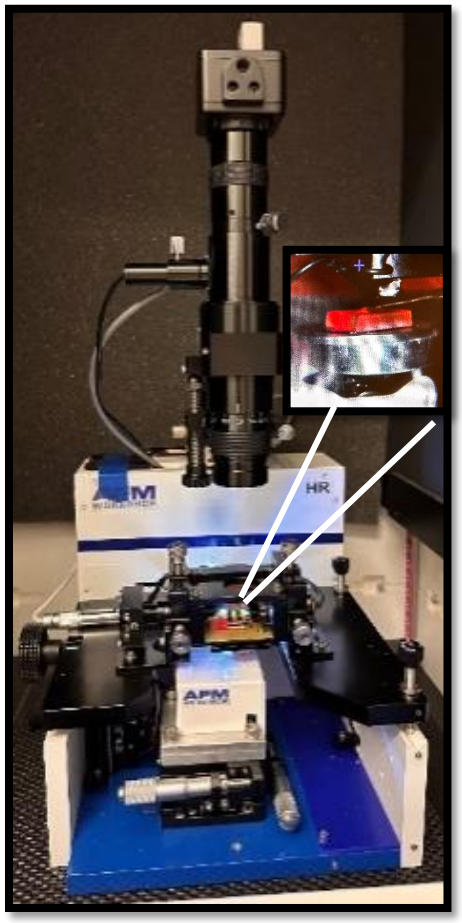

Figure 27. Atomic force microscope

CHAPTER III

RESULTS AND DISCUSSION

3.1. Confirmation of epoxidation and ring-opening synthesis

3.1.1. Iodine value

The iodine index is used to evaluate the unsaturation amount in sunflower oil. Unsaturation usually occurs mainly as double bonds in fatty acids of oil. 101 g I_2/100 g iodine value was determined for sunflower oil by the Hanus method, which indicates 0.39 moles of double bonds were available in 100 g of the sunflower oil. After the conversion of sunflower oil by epoxidation and ring-opening reaction, 0.01 g I_2/100 g was obtained as the iodine value for the polyol. This reduced iodine value of polyol suggests some amount of unsaturation content and a more reactive form of sunflower oil which can be utilized further for PU films' preparation.

3.3.2. Epoxy value

The oxirane number determines the epoxy content that existed in the substance. In this experiment, the epoxide value of ESFO to be 4.65% was determined. After the ring-opening reaction, the epoxy value was 0.01% for the polyol. This reduction in epoxide number after ring-opening reaction confirmed the transformation of epoxide sunflower oil into polyol.

3.3.3. Hydroxyl value

This value determines the functionality of polyol and the amount of isocyanate that is required for a chemical reaction to take place. For prepared SFO polyol, obtained hydroxyl value was 191 mg KOH/g. This value indicates the hydroxyl content in the polyol.

3.3.4. Fourier-transform infrared

FT-IR spectroscopy was used to determine the changes in chemical structures of SFO, ESFO, and SFO polyol. These changes can be specified by vanishing or shifting of absorption peaks as shown in **Figure 28**. The =C-H stretching of unsaturated carbons (H-C=C) was observed at 3005 cm^{-1}, in the spectra of SFO. The absence of this peak in ESFO indicates consumption of double bonds. A peak can be noticed at 832 cm^{-1} in ESFO spectra, which is due to the epoxy group (C-O-C) [55]. This peak confirmed the epoxidation process in this experiment. In the spectra of SFO polyol, a peak for (O-H) hydroxyl group stretching is observed at 3427 cm^{-1}. The ring-opening reaction can be confirmed by these peaks [56]. This test confirmed the successful synthesis of sunflower oil-based polyol.

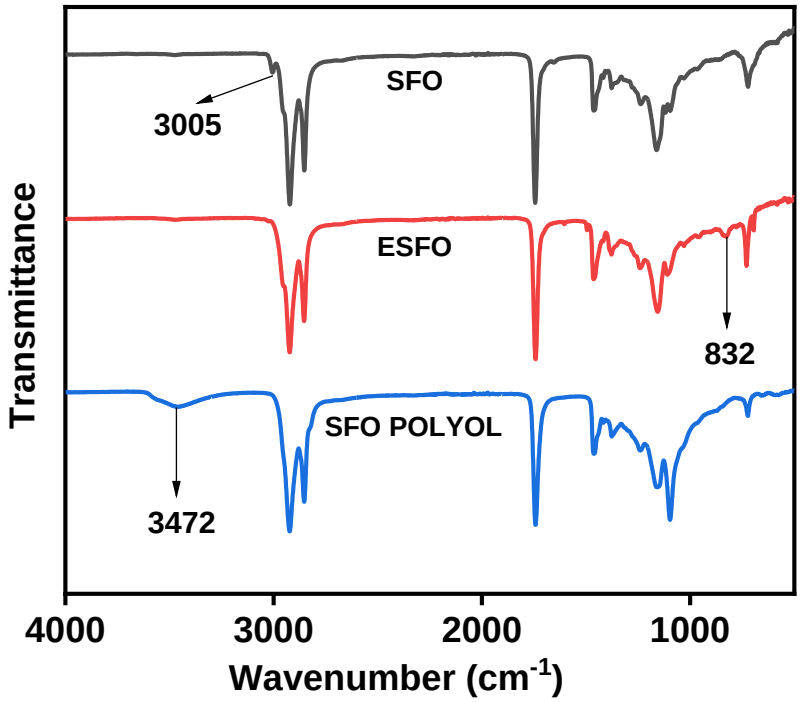

Figure 28. FT-IR results of SFO, ESFO and SFO polyol

3.3.5. Gel permeation chromatography

As an additional confirmative test, GPC was performed using SFO, EFSO, and SFO polyol. This is an analytical method in which the analytes separate according to sizes, through the columns. Smaller molecules can have longer time into the columns as they will enter easily via pores. On the contrary, bigger molecules only have a few pores to go in, consequently spending shorter time in columns. Due to this, solutions having smaller molecules show longer retention time compared to bigger molecules. As shown in **Figure 29**, the retention time is 23.2 minutes for SFO, 23.1 minutes for ESFO, and 22.7 minutes for SFO polyol. The retention time for SFO is a bit higher than the retention time of ESFO,

which can be due to the expected conversion of double bonds into the epoxy groups. These epoxy groups contain one oxygen atom that causes difference in the retention time. The retention time is lowest for SFO polyol which indicates an increment in molecular weight and further confirms the conversion of SFO to SFO polyol.

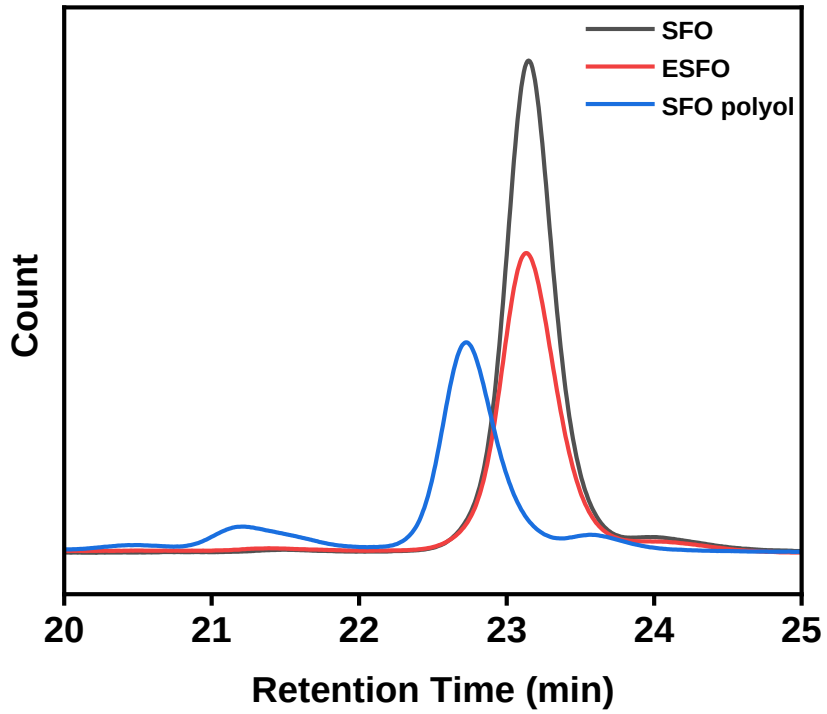

Figure 29. GPC of SFO, ESFO, and SFO polyol

3.3.6. Viscosity

Viscosity measurement plays an important role here because the processibility of the PUC films depends on it. Processing can be facile with low viscosity polyol as it causes an easy flow of polyol. The viscosity measured to be 0.069, 0.130, and 1.608 Pa.s for SFO, ESFO, and SFO polyol, respectively. The increment in the viscosity indicates the

increasing molecular weight from SFO to SFO polyol. This increment is also because of hydrogen bonding that corresponds to a higher amount of -OH groups present [57], which confirmed the transformation of SFO into the SFO polyol.

3.2. Confirmation of reinforcement materials

3.2.1. X-ray diffraction

XRD was used to determine the interlayer spacing and crystal structure of graphene-based fillers. To understand the structure of fillers, 2θ was recorded in between 10° to 80º. As shown in **Figure 30**, a peak appeared at 2θ = 26.6° in the XRD spectra of GNP with interlayer spacing of 3.35 A°, which indicates a higher quantity of stacked layers [58]. The spectra of GNR manifested a peak at 2θ = 26.8° that indicates an exfoliation and effective conversion of MWCNT to GNR [59]. The interlayer spacing was 3.32 A° [60]. The interlayer spacing was calculated according to Bragg's law:

$$n\lambda = 2d \sin\theta \quad \text{……. eq. (1)}$$

Where, n = diffraction order (n = 1)

λ = wavelength of used radiation ($Cu_{\propto}$ = 1.5406)

sin θ = diffraction angle

d = interlayer spacing

In the XRD spectra of rGO, a smaller broad peak can be noticed at 2θ = 24.1° due to the reduction of oxygenated groups in rGO and decreased distance among the graphitic layers [61]. The interlayer spacing is 3.69 A°. One more small peak is observed at 2θ =

42.6° (001) which is attributed as a turbostratic band of carbon-based compounds. Possibly, there is a combination of sp^2 and sp^3 hybridization states in the structure of carbon [61]. For GO filler, a sharp peak is observed at $2\theta = 26.6°$ that can be allocated to the (002) plane of graphite. The calculated interlayer spacing for the angle is 3.35 *A*°. This peak suggested the GO exfoliation, as it moved toward a lower angle than the (002) plane of graphite [62]. While comparing spectra of rGO and GO, a sharp peak at (002) is absent, indicating an amorphous nature of rGO. This interlayer spacing of all compounds perhaps correlate to the dispersion of them into the SFO polyol [63].

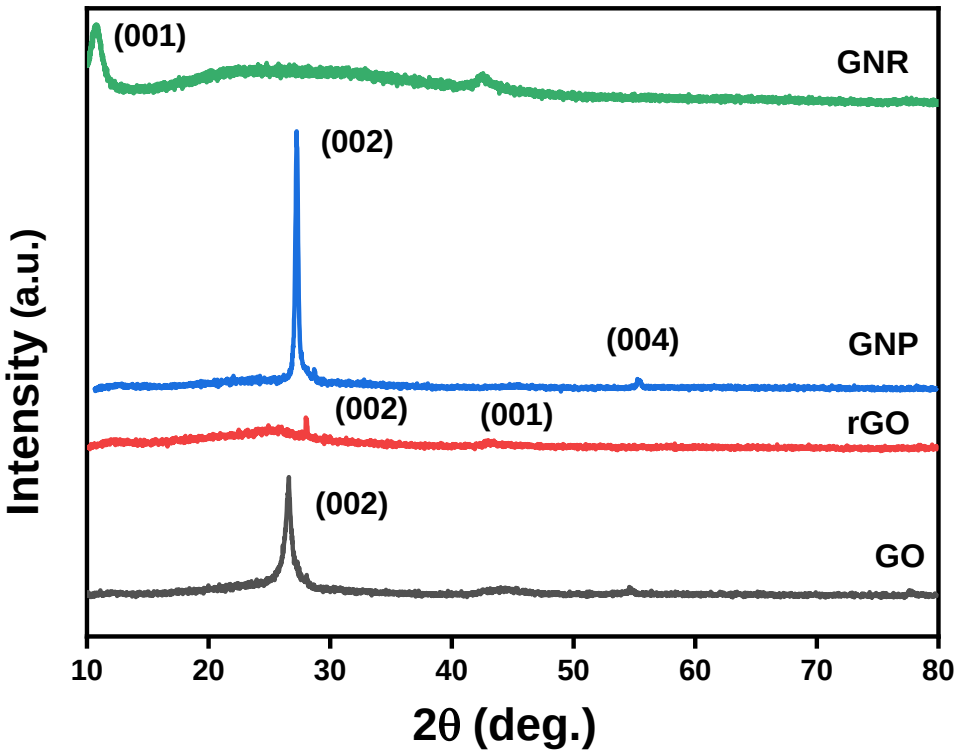

Figure 30. XRD spectra of GNR, GNP, rGO, and GO

3.3. Properties of the bio-based film

3.3.1. Thermogravimetric analysis

TGA was used for the analysis of thermal stability and thermal decomposition of the PUC films. TGA and DTGA as a function of weight (%) curves are shown in **Figure 31** for both PU/GNP and PU/GNR. TGA graph indicates two or three main peaks of weight loss of PUC. 5% weight loss is observed between 294-306 ^{o}C for all samples, as shown in **Table 2**. Between 387-397 ^{o}C, 50% weight loss of the PUC samples is mentioned. The peaks can be contributed to hard segments (HS) and soft segments (SS) of PU. Generally, decomposition of HS occurs at lower temperature and of SS occurs at higher temperature comparatively. This could be due to higher mobility of SS in the PU matrix. Apart from that, thermal stability is analyzed by comparing the residue percentages at 690 ^{o}C, which is increased from 1.4% of neat PU to 7.8% and 9% for the highest wt.% of GNP and GNR, respectively. In the case of GNP incorporation with PU, the enhanced thermal property could be due to the nature of interconnected GNP with PU that initiated barrier for heat prevention into the PUC samples [64]. On the other hand, GNR showed improvement that can be attributed to oxygen groups localized at the backbone of GNR, which further linked with hydrogen groups of PU chains by an effective hydrogen bonding. This linkage acted as a hindrance to avoid heat in the PUC films [43].

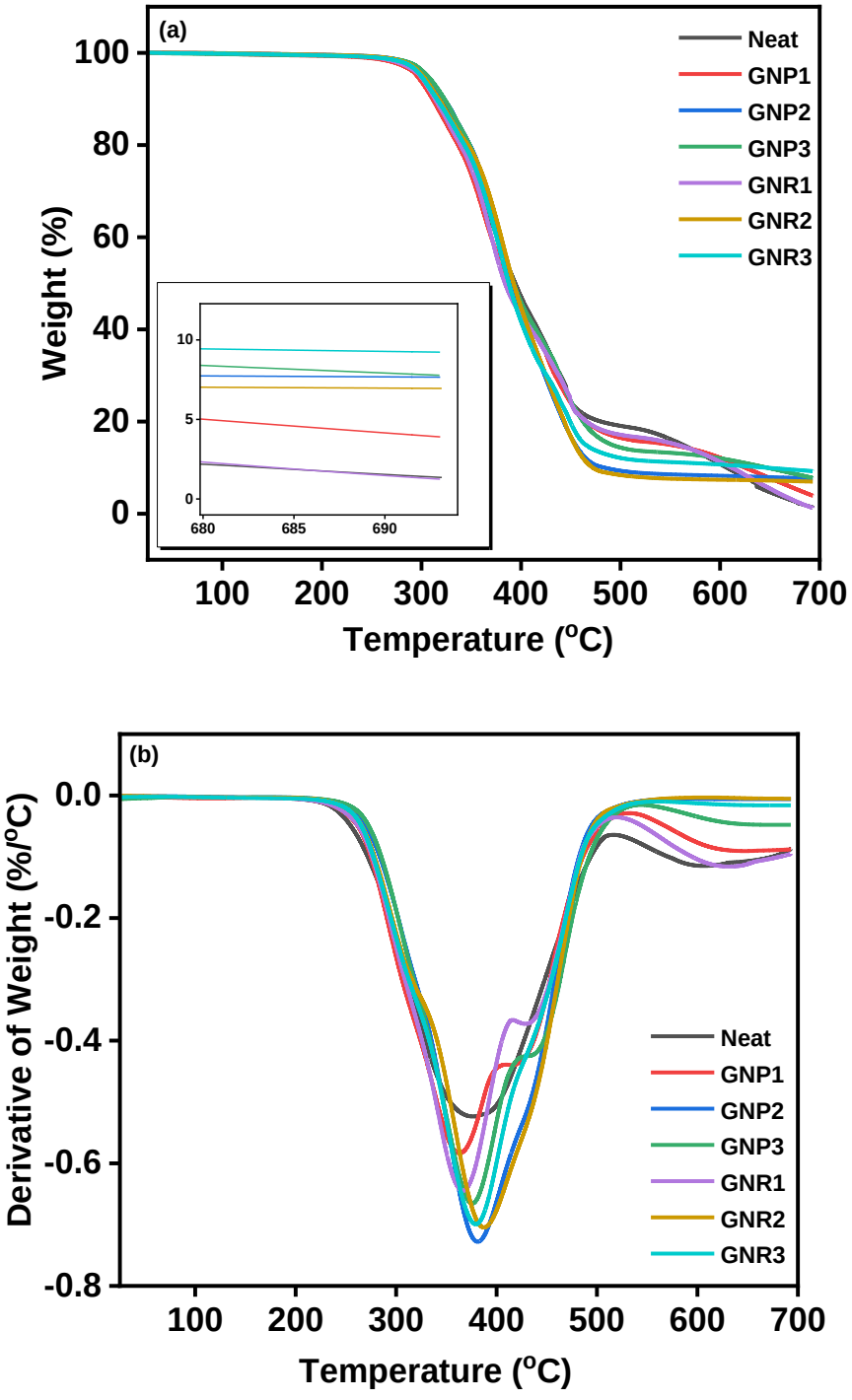

Figure 31. **(a)** TGA and **(b)** DTGA results of PUC having different amounts of GNP and GNR

For PU/rGO and PU/GO samples, a negligible enhancement in thermal stability was observed compared with the neat PU. Like the GNP and GNR samples, rGO and GO included PU samples that showed two or three stage decomposition (**Figure 32**). It is observed that increasing temperature promotes a lower mobility of the segments throughout the PU chains. For both rGO and GO, the highest char yield is observed at 690 ^{o}C for both rGO3 and GO3 with 9.6%. This could be due to more stability of fillers than PU [65,66].

Hence, graphene-based fillers allow effective heat transfer due to high thermal conductivity, which lowered the overheating of HS of PU. This way, fillers can provide thermal protection to the PU matrix as higher decomposition temperature was observed for PUC.

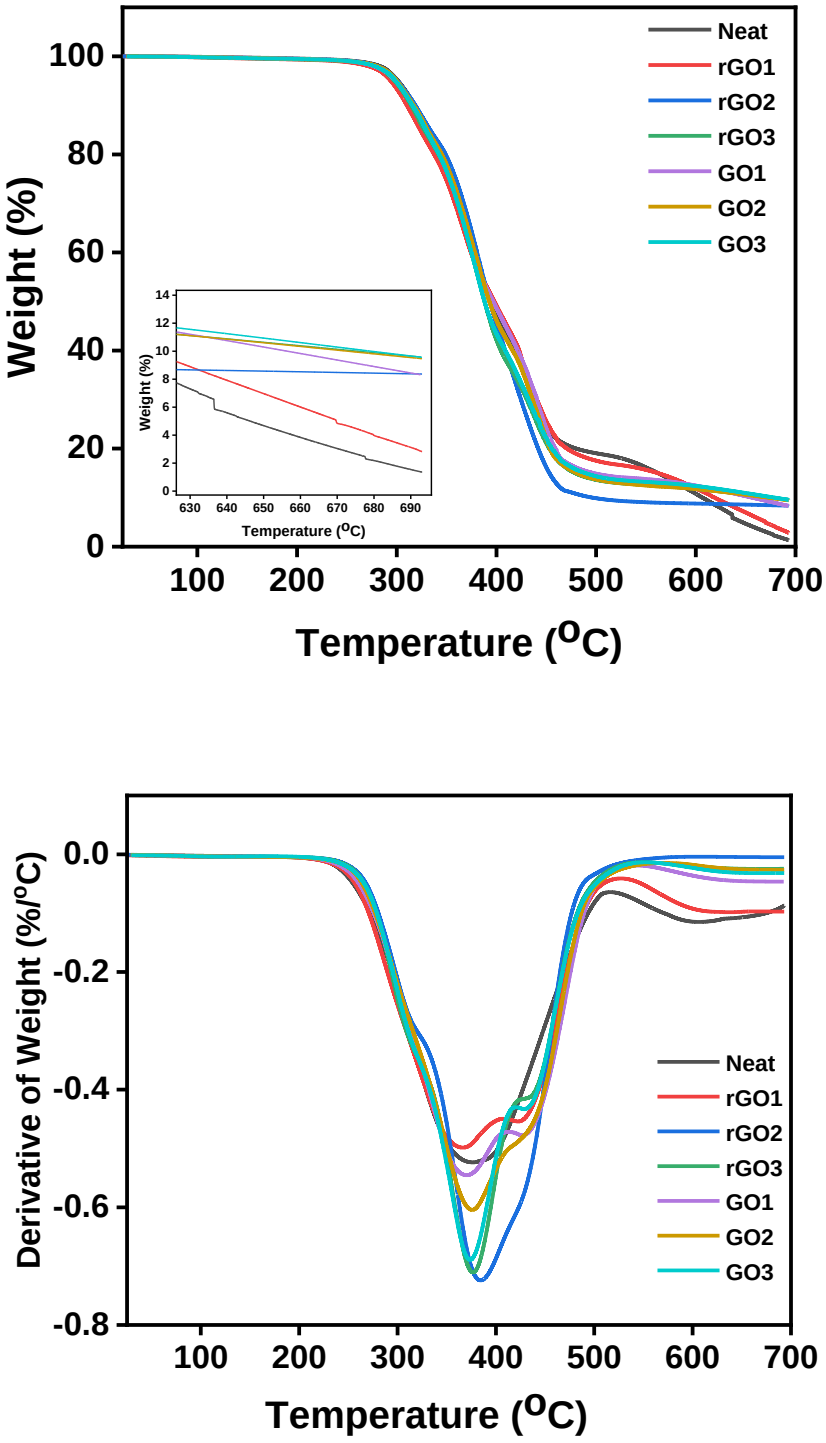

Figure 32. (a) TGA and **(b)** DTGA results of PUC having different amounts of rGO and GO

Table 2. TGA data for PUC samples

Sample	Temp. (ºC) at 5% weight loss	Temp. (ºC)at 50% weight loss	Weight (%) of ash remained at 690 ºC
Neat PU	301	344	1.4
GNP1	295	389	4.0
GNP2	304	390	7.7
GNP3	306	392	7.8
GNR1	298	383	1.3
GNR2	301	392	7.0
GNR3	299	387	9.2
rGO1	294	397	2.8
rGO2	300	393	8.4
rGO3	298	387	9.6
GO1	298	396	8.3
GO2	299	392	9.5
GO3	298	388	9.6

3.3.2. Differential scanning calorimetry

The DSC method was used to study the effect of fillers on the Tg the PUC. As shown in **Figure 33**, the Tg can be observed between 25-41 ºC for PUC. Specifically, Tg of neat PU is 33.75 ºC, whereas GNR2 and rGO2 has 25.63 ºC, 25.87 ºC, respectively. The Tg of GNP2 and GO2 was slightly higher than the neat PU, 40.01 ºC and 37.07 ºC, respectively. Tg results of DSC correlates with mechanical properties. The Tg point at room temperature, or lower than room temperature showed higher strain which means the material has little flexibility. On the other hand, materials which have a higher Tg than the room temperature for example, GNP2 and GO2 showed a brittle-nature.

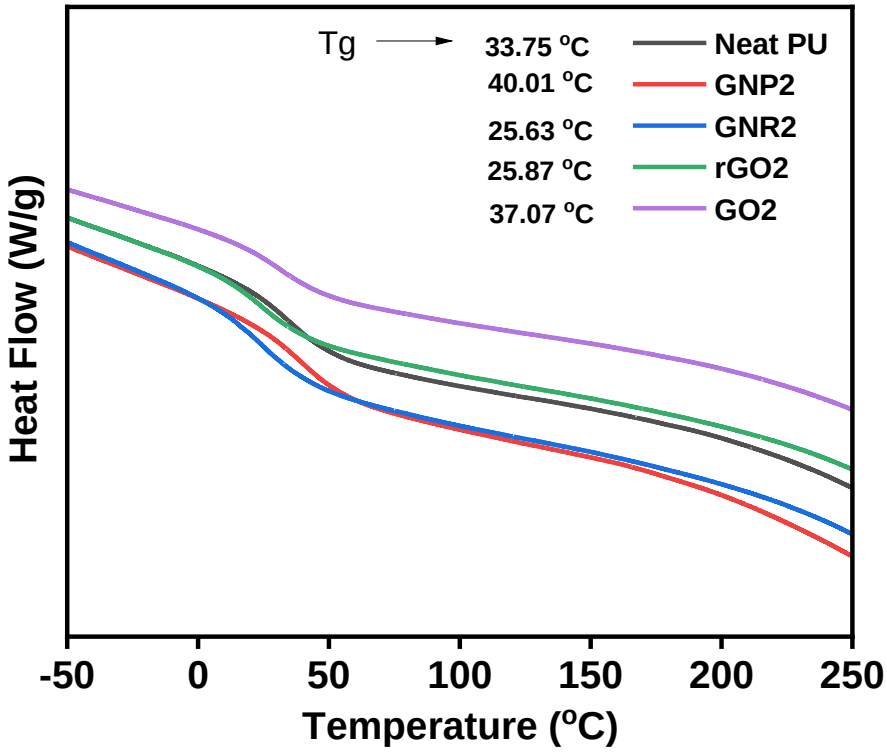

Figure 33. DSC result for PUC samples

3.3.3. Dynamic mechanical analysis

DMA is an essential mechanical technique to examine the storage modulus and the transition temperature (Tg) of the PUC films as shown in **Table 3**. **Figure 34** shows DMA graphs of storage modulus and Tg for both PU/GNP and PU/GNR. In the case of GNP addition to the PU, a storage modulus is higher than the neat PU for all wt.% of GNP, which is 430, 855, and 434 MPa for 0.01, 0.02, and 0.05 wt.% GNP, respectively. The improvement could be due to the reinforcement effect of GNP. A strong interlinkage between GNP and PU confined the motion of PU's molecular chains, and hence enhanced the storage modulus. Furthermore, the Tg is elevated continuously while increasing the

amount of GNP, which could be due to the chemical as well as physical interactions between functional groups of GNP and PU chains. When observing the tan delta, the Tg of GNP1 is 59 ℃, the Tg of GNP2 is 63.8 ℃, and the Tg of GNP3 is 64.3 ℃. Whereas Tg of neat PU is noticed at 49.2 ℃. On the flip side, PU/GNR shows a higher storage modulus than the neat PU for all wt.% of GNR, which is 368, and 419 MPa for 0.01, and 0.02 wt.% GNR, respectively. This result could be attributed to a synergistic effect of the phase segregation and insertion of GNR. Moreover, the Tg of GNR1 is 50.5 ℃, the Tg of GNR2 is 41.0 ℃, and the Tg of GNR3 is 40.5 ℃. This could be because of PU's phase segregation that included soft segments connected with hard segments, providing a smooth movement of the soft segments [67].

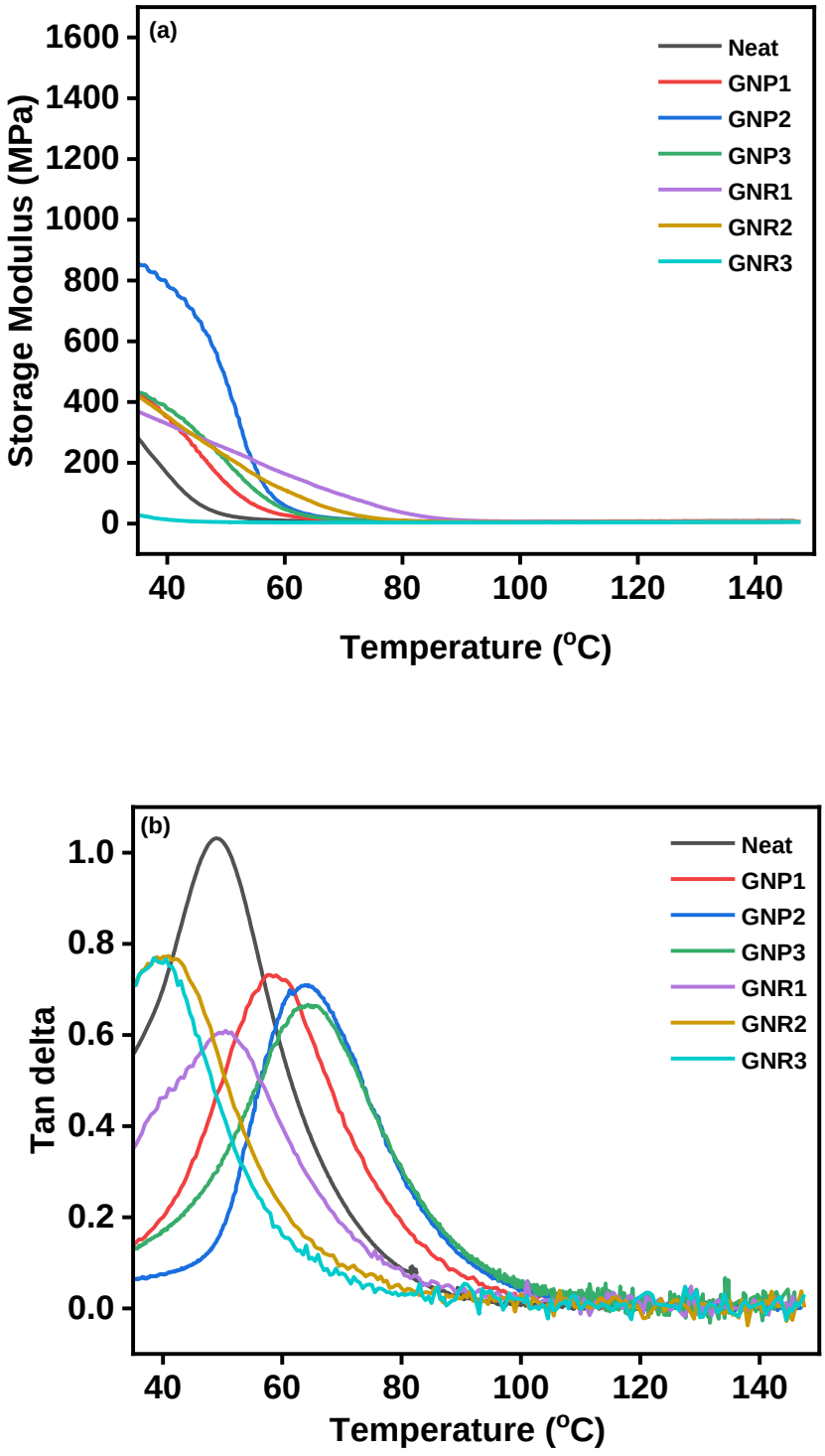

Figure 34. (a) Storage modulus and **(b)** tan delta of PU/GNP and PU/GNR

The storage modulus and tan δ presented in **Figure 35** for both PU/rGO and PU/GO. The storage modulus for rGO1, rGO2 and rGO3 is 466, 516 and 482 MPa, respectively. The maximum tan δ presents the Tg point for PU/rGO films. rGO1, rGO2, and rGO3 showed Tg of 53.3, 50.6, and 51.8 ℃, respectively. This declining Tg values of rGO could be because of less oxygenated groups in rGO that show a weak interaction with hard segments, likely decreasing the crosslinking density of the polymer structure [68]. The GO included sample showed the highest storage modulus of 1316 MPa for 0.05 wt.% amount, which is almost double the neat PU. For 0.02 wt.% amount of GO, the storage modulus is decreased to 725 MPa from 1316 MPa. GO1 has a storage modulus of 368 MPa. In terms of Tg, all concentrations of GO insertion showed higher results compared to the neat PU. This increment in Tg could be due to the movement of polymer chains hindered by GO nanosheets by a lamellar barrier effect. Thus, the required energy to flow the polymeric chains was higher [68].

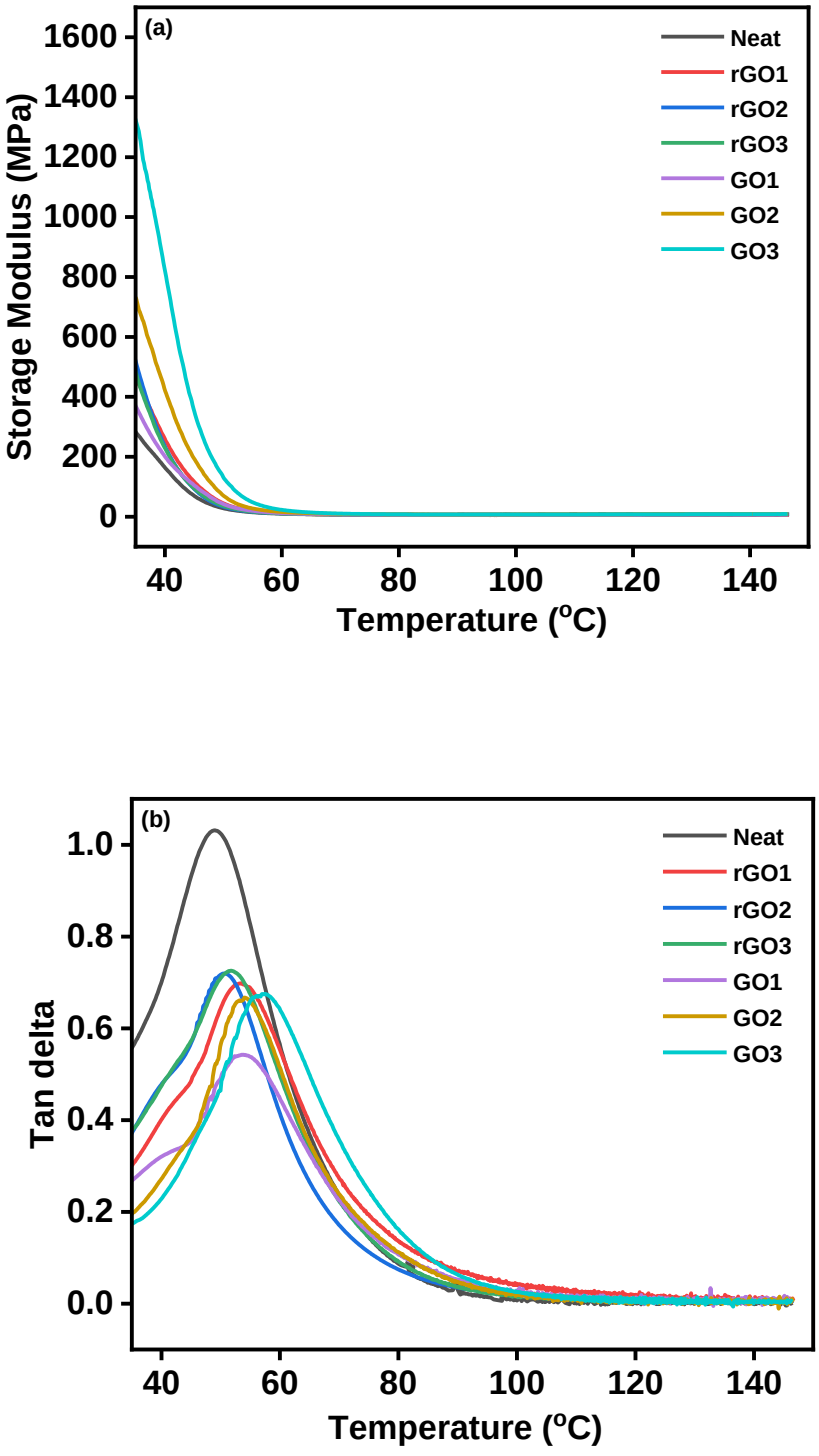

Figure 35. (a) Storage modulus and **(b)** tan delta of PU/rGO and PU/GO

Table 3. DMA data of storage modulus and Tan delta

Sample	Storage Modulus (MPa)	Tg (°C)
Neat PU	283	49.2
GNP1	430	59.0
GNP2	855	63.8
GNP3	434	64.3
GNR1	368	50.5
GNR2	419	41.0
GNR3	028	40.5
rGO1	466	53.3
rGO2	516	50.6
rGO3	482	51.8
GO1	368	53.7
GO2	725	54.3
GO3	1316	57.4

3.3.4. Tensile strength

Tensile test was the foremost mechanical method used to study the mechanical strength of the PUC films. The films were mechanically strengthened by adding graphene-based fillers. While analyzing **Figure 36 (a)**, the tensile strength for neat PU film was 9.47 MPa whereas, the tensile stress of 31.8, 26.7, and 34.9 MPa was observed for GNP1, GNP2, and GNP3, respectively. Uniform dispersion of GNP can be confirmed in the backbone of PU up to the 0.02 wt.% concentration of GNP. This led to a continuous increment in the tensile strength that could be due to chemical bonding and physical interconnection of functional groups of GNP and PU chains. The tensile strength was decreased while adding a higher amount of GNP into the PU which can be attributed to aggregation. Hence, GNP filler is assisting the tensile strength increment that corresponds to the stiffness of PUC. In the case of GNR filler, the tensile strength was enhanced from

9.47 (neat PU) to 13.9 MPa for GNR1, while 10.4 MPa for GNR2. Differentiating GNR3 sample, 8.2 MPa tensile strength was obtained. The enhancement of mechanical properties until 0.02 wt. % GNR addition could be because of the inter-filler gap which is far enough and the polymeric chain amount between filler particles is sufficiently large to generate strong filler-polymer interlinkage, which shows effective load-transfer manner. However, the load-transfer was poor for the GNR3 sample, resulting in a lower tensile strength [60].

As shown in **Figure 36 (b)**, the rGO filler addition to the PU caused an increment in the yield at the break. The tensile stress yield is slightly more increased than the neat PU film (9.47 MPa) and obtained around 11 MPa for rGO1 and rGO2 whereas it is 14 MPa for rGO3. This type of mechanical behavior could be due to a good interaction of rGO with soft segments; hence, PU/rGO films are indeed flexible and caused more mobility to the polymer chains [69]. In this way, the tensile property of PU/rGO films went from tough to more flexible. Opposed to rGO, the addition of GO filler into the PU films presented low tensile strain and high stress, meaning tougher to more brittle behavior from neat to PU/GO films. 0.01 wt.% addition of GO filler caused a significant decrement compared to the neat PU film. This decrement can be due to a smaller concentration of GO that generates disturbance of the polymer chains and stimulates some microphase separation. Moreover, 0.02 and 0.05 wt.% filler addition that showed 32.5 and 26 MPa tensile stress at yield, respectively. Specific behavior can be due to the interconnection by the hydrogen bonding between the oxygenated groups of GO with aminic hydrogen from the urethane linkage. The decrement for 0.05 wt. % of GO into the PU matrix is due to GO sheets which tend to come closer to each other and create aggregation because of the string Vander wall force.

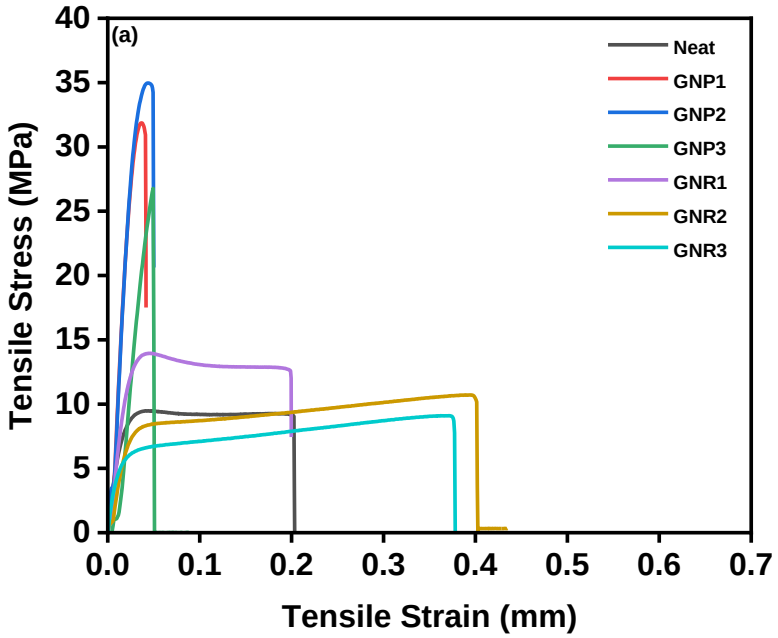

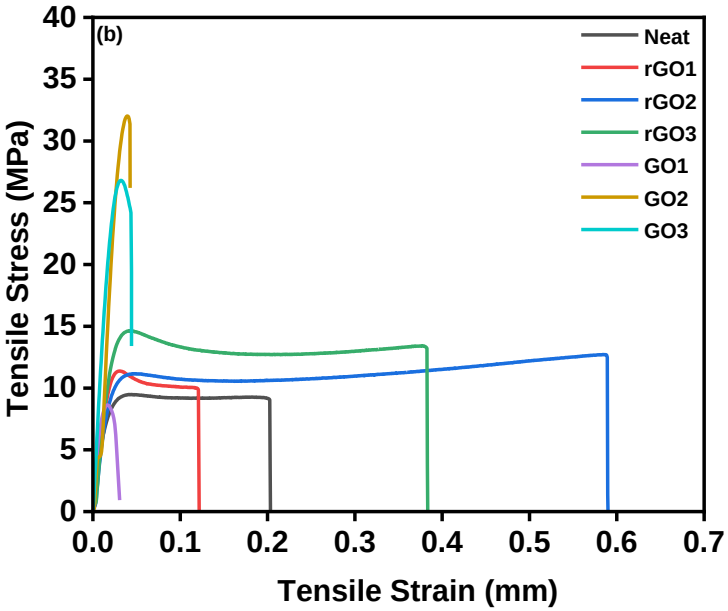

Figure 36. Tensile strength of PU having different amounts of **(a)** GNP and GNR, and **(b)** rGO and GO

3.3.5. Three-point flexural test

Load (N) vs. extension (mm) curves are shown in **Figure 37** to determine the flexural strength of PUC films. For GNP-filler-inserted PU films, the flexural strength was considerably upgraded and extended more than 6 N for 0.01 wt.% GNP and 0.02 wt.% GNP loading to PU. The flexural strength decreased further for 0.05 wt.% GNP yet showed more than the neat PU film (2.3 N) [70]. Meanwhile, the incorporation of GNR filler with PU films shows a higher result than the neat film in terms of extension which was more than 16 mm. The flexural result of PU/GNR films is also matched with tensile strength result [71].

In the study of PU/rGO films, 0.02 wt.% addition of rGO allowed a significant enhancement with a load of 14 N and an extension of 10.5 mm in the PUC films. On the flip side, the reduction in flexural property can be observed with 0.01 and 0.05 wt.% incorporation of rGO with PU films. Observing PU/GO films, the flexural strength was improved for 0.02 wt.% addition of GO which was 5 N and 8 mm, although flexural strength for higher amount addition yielded almost same as the neat PU film.

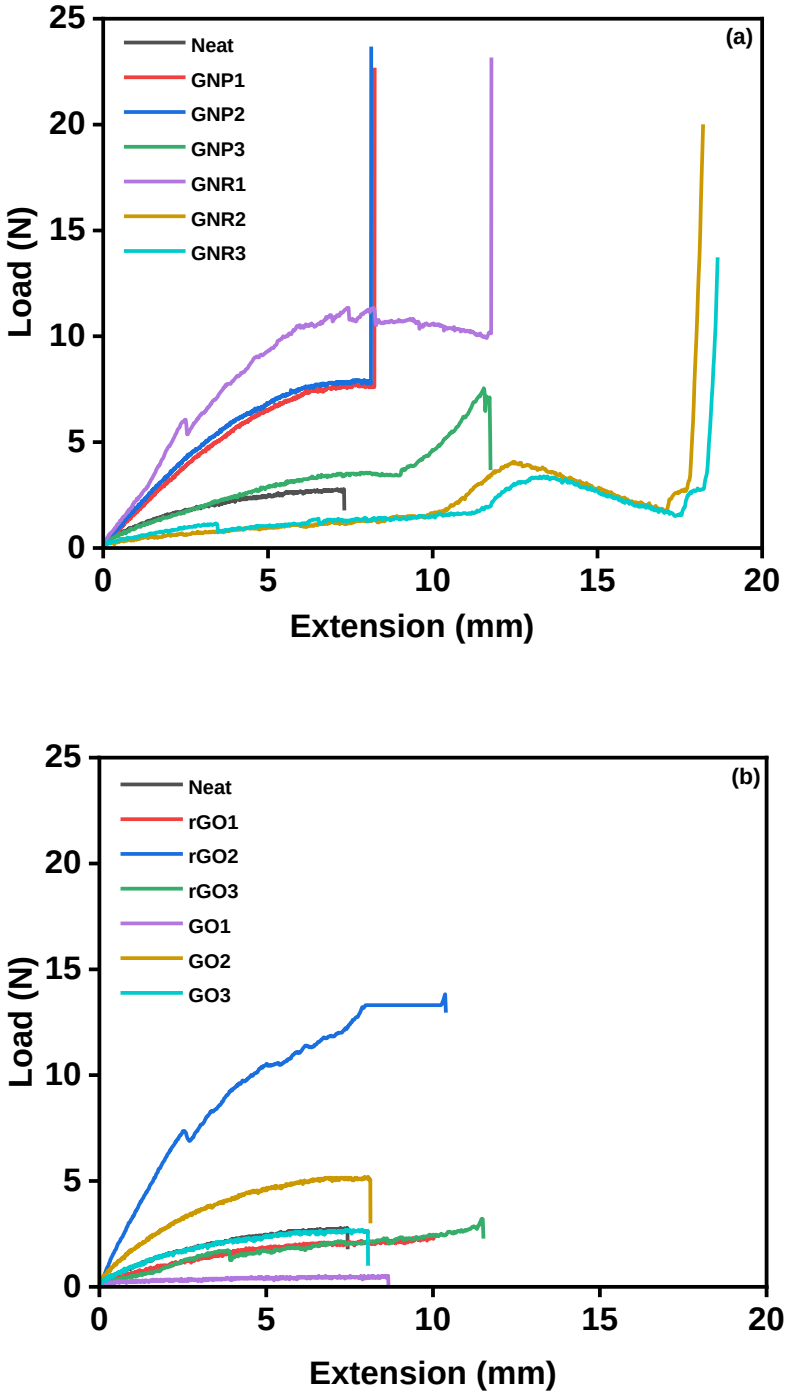

Figure 37. Flexural strength of PU having different amounts of **(a)** GNP and GNR, and **(b)** rGO and GO

3.3.6. Hardness

The hardness of PUC films was measured with scale D as it is suitable for harder materials. Three films of each type of sample were measured for average. As shown in **Figure 38**, the hardness for all PUC films was higher than the neat PU film that has a shore D value of 51. In the case of PU/GNP films, the hardness was the highest among all fillers which increased continuously from a smaller to a higher concentration of GNP, with the highest result of 70 shore D. This outcome can be due to the interaction between GNP and PU as described by tensile strength [72]. For GNR-based PUC films, the hardness results are contradictory. The hardness study showed decrement with increasing concentration of GNR, although it was higher than the neat PU film. On the other hand, the highest concentration of rGO combined with PU film offered a hardness of 60 shore D, which could be interactions of rGO nanosheets with the soft segments as they have similar polarity [73]. In the case of GO assembled with PU film, shore D hardness of 67 was observed because of the interaction of presented oxygenated groups of GO with the urethane linkage [74].

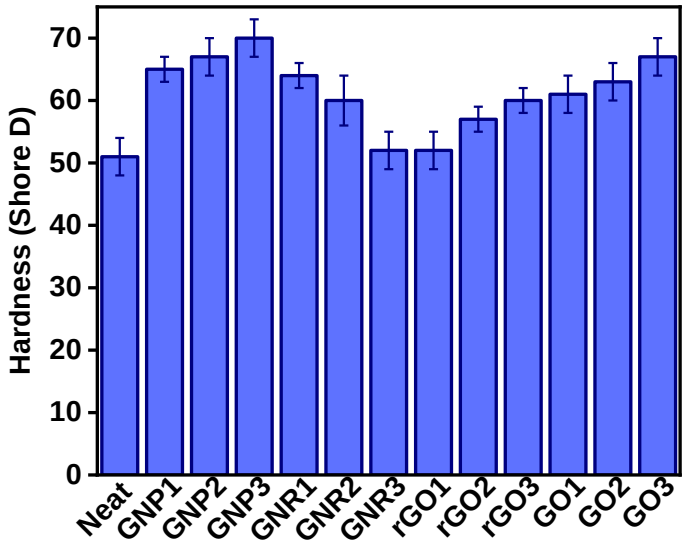

Figure 38. The hardness of PUC films

3.3.7. Water contact angle

The wettability of the film plays an important role in film applications like corrosion resistance, self-cleaning and anti-icing. The WCAs were obtained by using a water droplet placed on the film's surface. An average of five measurements of WCAs accounted for results. As shown in **Figure 39**, the WCA was 72.87° for the neat PU film, which was increased upon adding graphene-based fillers. In the case of the highest GNP concentration, the obtained WCA was 91.21° which was almost 18° higher than the neat PU. This transition from hydrophilic to hydrophobic could be due to denser morphology and insufficient vacant sites in PU/GNP that diminished the water transmit through the PUC film [75]. Similar improvement in WCA can be observed in PU/GNR films. 92.38° was the WCA for the highest amount's introduction of GNR into the PU film. This could be because of the introduction of GNR that customized the morphology and GNR's

hydrophobic nature [76,77]. Digital images of neat PU and PU/GNP sample are shown in **Figure 40**.

For GO and for rGO-containing PU films, WCA of PU/GO films decreased slightly yet was higher than the neat PU film. This can be attributed to the functional groups present in GO, such as carboxyl and hydroxyl, that modify it and show hydrophilic nature. Among all used graphene-based fillers, rGO-containing PU film shows higher WCA of 104.22° by 0.05 wt.% addition. rGO has more limited functional groups than GO, hence shows enhanced WCA of PUC films [78].

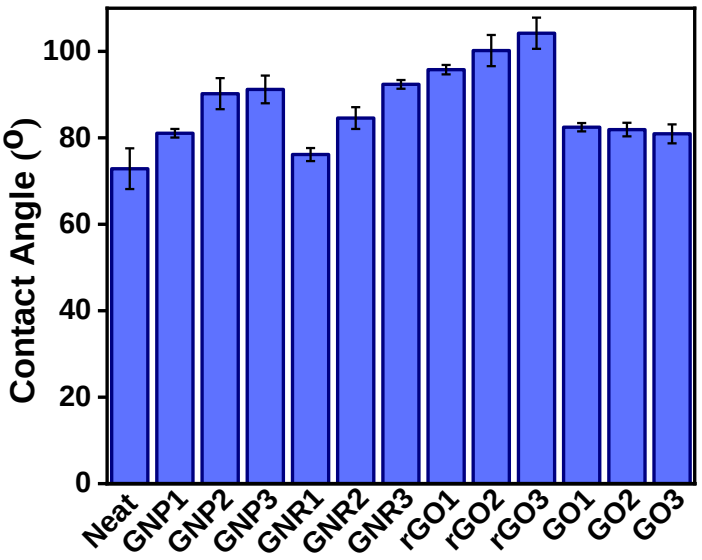

Figure 39. WCA of PUC films

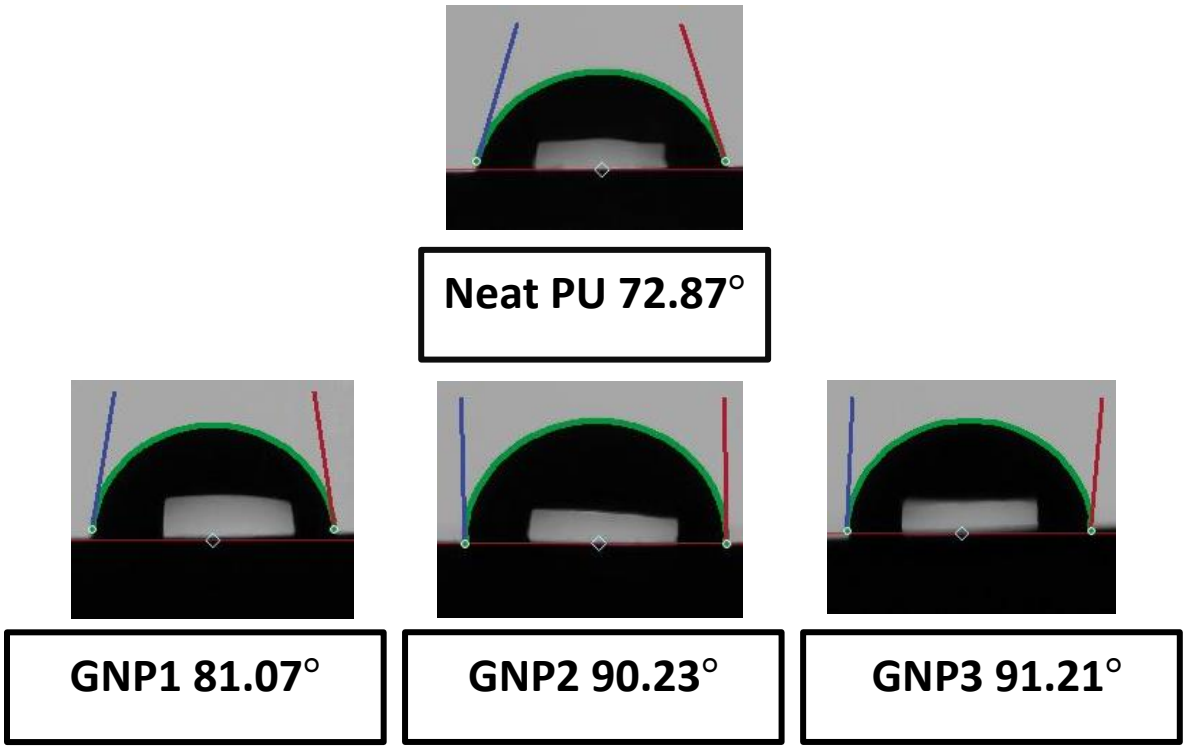

Figure 40. Images of WCA for PUC

3.3.8. Atomic force microscopy

AFM images were used to study the morphology of the PUC films. **Figure 41** shows 3D images and **Table 4** shows roughness data of the neat PU film along with PUC films. The images were studied in terms of roughness of the samples. The roughness of the neat PU was 15.08 nm. It can be observed that the roughness was increased for the 0.02 wt.% fillers included films. For example, GO2 sample has roughness of 28.16 nm, whereas roughness of rGO was 16.56 nm. This can be because of the height of strips-like structure that can be noticed on the surface of PUC films. However, for the lowest and highest concentrations of the fillers, the roughness was relatively lower than 0.02 wt.% containing fillers. The roughness of GNP1 was 13 nm [79].

Table 4. Surface roughness of PUC films

Sample	Roughness (nm)
Neat PU	15.08
GNP1	13.00
GNP2	15.98
GNP3	7.49
GNR1	10.03
GNR2	9.10
GNR3	11.40
rGO1	3.36
rGO2	16.56
rGO3	4.50
GO1	3.98
GO2	28.16
GO3	2.09

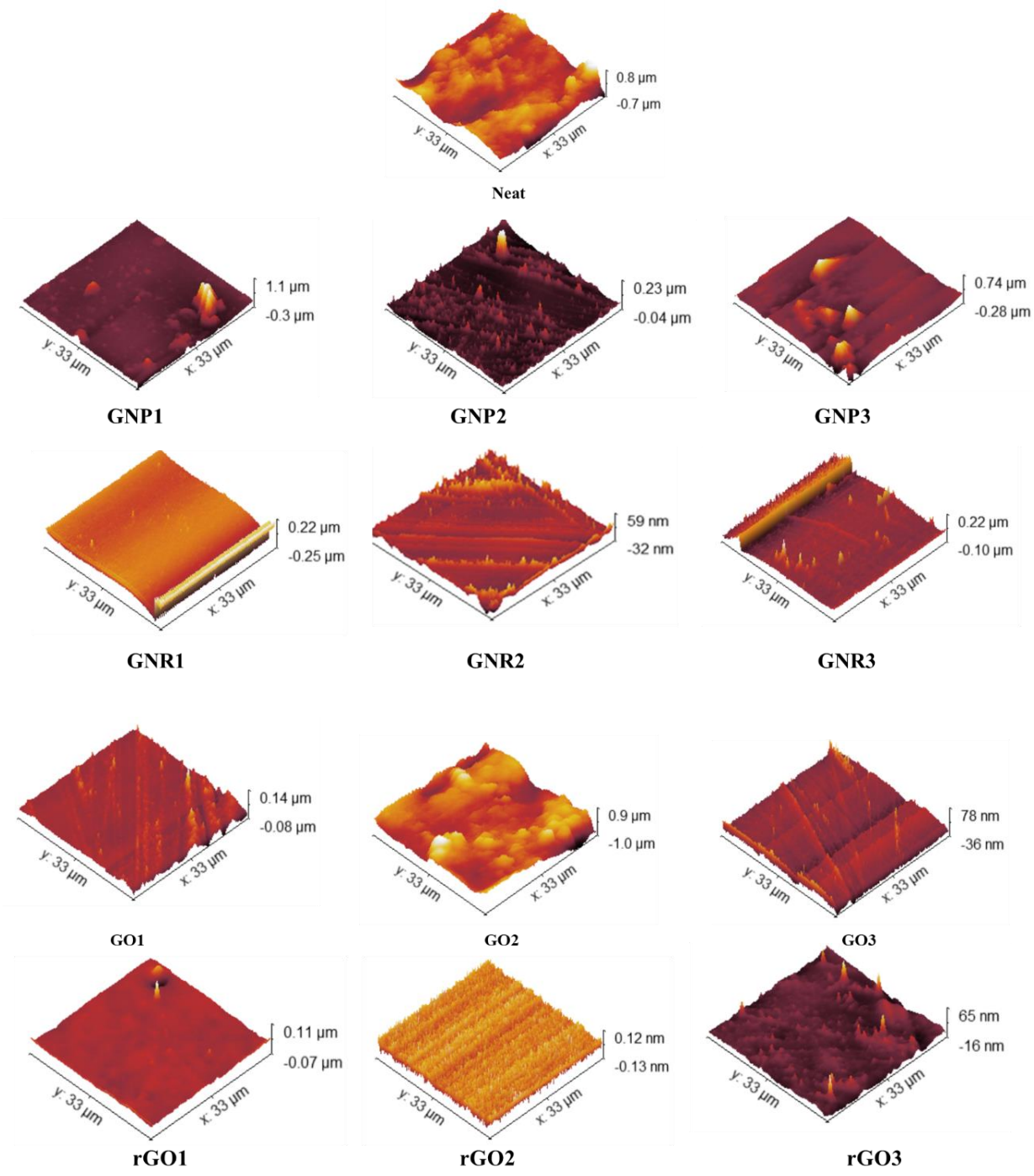

Figure 41. AFM images of PUC films

CHAPTER IV

CONCLUSION

The investigation of renewable resources to produce PU is currently an interesting and valuable research topic. In this project, the utilization of sunflower oil to produce polyol was studied by following the epoxidation and ring-opening method. Polyol was characterized by FT-IR and GPC techniques. Thermal and mechanical strength were enhanced by introducing graphene-based fillers like GNP, GNR, rGO and GO.

In terms of thermal stability, the amount of residue percentage was increased for PUC samples. In DSC testing, the highest Tg of 40.01 ℃ was obtained for GNP2 sample. Moreover, the storage modulus was increased due to the addition of fillers and the highest was obtained 1316 MPa for 0.05 wt.% GO. Also, the observed Tg from tan delta curve matches the result of DSC data. The maximum tensile strength was observed by GNP2 sample which was 34.9 MPa. All GNR and rGO containing films showed higher strain behavior. A three-point flexural test was performed to study the flexural strength of PUC films, where the highest flexural strength was around 14 MPa for 0.02 wt.% rGO sample. Furthermore, the hardness of the PUC films was measured by indentation; GNP3 has the highest shore D hardness of 70 D. The wettability and surface morphology were examined by WCA and AFM tests, respectively. A hydrophobicity can be observed in few samples in which, a 104.22° angle was the highest for rGO3 sample. Microscopy was used to

analyze the roughness of the films. The roughness was increased upon adding fillers. In short, sunflower oil deserves consideration as a raw material for the preparation of PUC films.

REFERENCES

[1] H.W. Engels, H.G. Pirkl, R. Albers, R.W. Albach, J. Krause, A. Hoffmann, H. Casselmann, J. Dormish, Polyurethanes: Versatile materials and sustainable problem solvers for today's challenges, Angew. Chemie - Int. Ed. 52 (2013) 9422–9441.

[2] R. Jayakumar, S. Nanjundan, M. Prabaharan, Metal-containing polyurethanes, poly(urethane–urea)s and poly(urethane–ether)s: A review, React. Funct. Polym. 66 (2006) 299–314.

[3] J. Brzeska, A. Piotrowska-Kirschling, A brief introduction to the polyurethanes according to the principles of green chemistry, Processes. 9 (2021) 1929.

[4] J.O. Akindoyo, M.D.H. Beg, S. Ghazali, M.R. Islam, N. Jeyaratnam, A.R. Yuvaraj, Polyurethane types, synthesis and applications-a review, RSC Adv. 6 (2016) 114453–114482.

[5] V. Mahendra, Eco-foams from pine resins A report on the works of foaming methodologies from pine resins, 3 (2016) 1–22.

[6] M. Ghozali, E. Triwulandari, A. Haryono, Preparation and Characterization of Polyurethane-Modified Epoxy with Various Types of Polyol, Macromol. Symp. 353 (2015) 154–160.

[7] G. Atiwesh, A. Mikhael, C.C. Parrish, J. Banoub, T.A.T. Le, Environmental impact of bioplastic use: A review, Heliyon. 7 (2021) e07918.

[8] J. Konieczny, K. Loos, Green polyurethanes from renewable isocyanates and biobased white dextrins, Polymers (Basel). 11 (2019) 256.

[9] A. Stohl, Z. Klimont, S. Eckhardt, K. Kupiainen, V.P. Shevchenko, V.M. Kopeikin, A.N. Novigatsky, Black carbon in the Arctic: The underestimated role

of gas flaring and residential combustion emissions, Atmos. Chem. Phys. 13 (2013) 8833–8855.

[10] Y. Lu, R.C. Larock, Soybean-oil-based waterborne polyurethane dispersions: Effects of polyol functionality and hard segment content on properties, Biomacromolecules. 9 (2008) 3332–3340.

[11] S. Gryglewicz, W. Piechocki, G. Gryglewicz, Preparation of polyol esters based on vegetable and animal fats, Bioresour. Technol. 87 (2003) 35–39.

[12] R.A. Talja, H. Helén, Y.H. Roos, K. Jouppila, Effect of various polyols and polyol contents on physical and mechanical properties of potato starch-based films, Carbohydr. Polym. 67 (2007) 288–295.

[13] H. Tian, Y. Wang, L. Zhang, C. Quan, X. Zhang, Improved flexibility and water resistance of soy protein thermoplastics containing waterborne polyurethane, Ind. Crops Prod. 32 (2010) 13–20.

[14] L. Hojabri, X. Kong, S.S. Narine, Fatty Acid-Derived diisocyanate and biobased polyurethane produced from vegetable oil: Synthesis, polymerization, and characterization, Biomacromolecules. 10 (2009) 884–891.

[15] S.B. Murmu, Alternatives derived from renewable natural fibre to replace conventional polyurethane rigid foam insulation, Clean. Eng. Technol. 8 (2022) 100513.

[16] S. Sahoo, S. Mohanty, S.K. Nayak, Biobased polyurethane adhesive over petroleum based adhesive: Use of renewable resource, J. Macromol. Sci. Part A Pure Appl. Chem. 55 (2018) 36–48.

[17] N. Mahmood, Z. Yuan, J. Schmidt, C. Xu, Preparation of bio-based rigid

polyurethane foam using hydrolytically depolymerized Kraft lignin via direct replacement or oxypropylation, Eur. Polym. J. 68 (2015) 1–9.

[18] P.M. Paraskar, M.S. Prabhudesai, R.D. Kulkarni, Synthesis and characterizations of air-cured polyurethane coatings from vegetable oils and itaconic acid, React. Funct. Polym. 156 (2020) 104734.

[19] J.A. Callow, S.A. Crawford, M.J. Higgins, P. Mulvaney, R. Wetherbee, The application of atomic force microscopy to topographical studies and force measurements on the secreted adhesive of the green alga Enteromorpha, Planta. 211 (2000) 641–647.

[20] P.M. Paraskar, M.S. Prabhudesai, V.M. Hatkar, R.D. Kulkarni, Vegetable oil based polyurethane coatings – A sustainable approach: A review, Prog. Org. Coatings. 156 (2021) 106267.

[21] R. Wang, T. Xiang, W.F. Zhao, C.S. Zhao, A facile approach toward multi-functional polyurethane/polyethersulfone composite membranes for versatile applications, Mater. Sci. Eng. C. 59 (2016) 556–564.

[22] B. V Tawade, R.D. Shingte, S.S. Kuhire, N. V Sadavarte, K. Garg, D.M. Maher, A.B. Ichake, A.S. More, P.P. Wadgaonkar, Bio-Based Di-/Poly-isocyanates for Polyurethanes: An Overview, PU Today. 4 (2017) 41–46.

[23] I. Javni, D.P. Hong, Z.S. Petrovič, Polyurethanes from soybean oil, aromatic, and cycloaliphatic diamines by nonisocyanate route, J. Appl. Polym. Sci. 128 (2013) 566–571.

[24] M. Mohamed, S. Hawkins, K. Chandrashekhara, Manufacturing and performance evaluation of polyurethane composites using one-part and two-part resin systems,

Polym. Polym. Compos. 23 (2015) 333–344.

[25] A.K. Mazitova, I.I. Zaripov, G.K. Aminova, M. V. Ovod, N.L. Suntsova, Fillers for polymer composite materials, Nanotechnologies Constr. 14 (2022) 294–299.

[26] M. Xanthos, R.N. Rothon, O. Access, C. Burgoyne, V. Ambrogi, C. Carfagna, P. Cerruti, V. Marturano, Part I Polymers and Fillers, Macromolecules. 12 (2016) 2171–83.

[27] A. Soundhar, M. Rajesh, K. Jayakrishna, M.T.H. Sultan, A.U.M. Shah, Investigation on mechanical properties of polyurethane hybrid nanocomposite foams reinforced with roselle fibers and silica nanoparticles, Nanocomposites. 5 (2019) 1–12.

[28] M. Tawfik, N. Ahmed, A. Ward, Characterization of kaolin-filled polymer composites, 8 (2013) 40–42.

[29] Q. Ma, J. Zhu, Research on structure and performance of polyurethane elastomer/superfine talcum powder composite, IOP Conf. Ser. Earth Environ. Sci. 558 (2020) 32039.

[30] S. Stankovich, D.A. Dikin, G.H.B. Dommett, K.M. Kohlhaas, E.J. Zimney, E.A. Stach, R.D. Piner, S.B.T. Nguyen, R.S. Ruoff, Graphene-based composite materials, Nature. 442 (2006) 282–286.

[31] M. Moshinsky, Final Report: Atomic Scale Imaging of the Electronic Structure and Chemistry of Graphene and its Precursors on Metal Surfaces, Nucl. Phys. 13 (1959) 104–116.

[32] J. Ortiz Balbuena, P. Tutor De Ureta, E. Rivera Ruiz, S. Mellor Pita, Enfermedad de Vogt-Koyanagi-Harada, Med. Clin. (Barc). 146 (2016) 93–94.

[33] S.K. Tiwari, S. Sahoo, N. Wang, A. Huczko, Graphene research and their outputs: Status and prospect, J. Sci. Adv. Mater. Devices. 5 (2020) 10–29.

[34] Stuart Milne, Mechanised Exfoliation Process for the Production of Graphene, (2015) 1–6. https://www.azonano.com/article.aspx?ArticleID=4066.

[35] M.R. Akkaya, Prediction of fatty acid composition of sunflower seeds by near-infrared reflectance spectroscopy, J. Food Sci. Technol. 55 (2018) 2318–2325.

[36] P.M. Rosa, R. Antoniassi, S.C. Freitas, H.R. Bizzo, D.L. Zanotto, M.F. Oliveira, V.B.R. Castiglioni, Chemical composition of brazilian sunflower varieties, Helia. 32 (2009) 145–156.

[37] T. Balakrishnan, S. Sathiyanarayanan, S. Mayavan, Advanced Anticorrosion Coating Materials Derived from Sunflower Oil with Bifunctional Properties, ACS Appl. Mater. Interfaces. 7 (2015) 19781–19788.

[38] S.T. McKenna, T.R. Hull, The fire toxicity of polyurethane foams, Fire Sci. Rev. 5 (2016) 1–27.

[39] R.W. Kapp, Isocyanates, Encycl. Toxicol. Third Ed. 2 (2014) 1112–1131.

[40] P. Cataldi, applied sciences Graphene Nanoplatelets-Based Advanced Materials and Recent Progress in Sustainable Applications, Appl. Sci. 8 (2018) 1438.

[41] P. Costa, J. Nunes-Pereira, J. Oliveira, J. Silva, J.A. Moreira, S.A.C. Carabineiro, J.G. Buijnsters, S. Lanceros-Mendez, High-performance graphene-based carbon nanofiller/polymer composites for piezoresistive sensor applications, Compos. Sci. Technol. 153 (2017) 241–252.

[42] A. Kausar, Graphene nanoribbon: fundamental aspects in polymeric nanocomposite, Polym. Technol. Mater. 58 (2019) 579–596.

[43] S. Shang, L. Gan, C.W.M. Yuen, S.X. Jiang, N.M. Luo, The synthesis of graphene nanoribbon and its reinforcing effect on poly (vinyl alcohol), Compos. Part A Appl. Sci. Manuf. 68 (2015) 149–154.

[44] A. Vasudevan, V. Shvalya, A. Zidanšek, U. Cvelbar, Tailoring electrical conductivity of two dimensional nanomaterials using plasma for edge electronics: A mini review, Front. Chem. Sci. Eng. 13 (2019) 427–443.

[45] R. Tarcan, O. Todor-Boer, I. Petrovai, C. Leordean, S. Astilean, I. Botiz, Reduced graphene oxide today, J. Mater. Chem. C. 8 (2020) 1198–1224.

[46] A.T. Smith, A.M. LaChance, S. Zeng, B. Liu, L. Sun, Synthesis, properties, and applications of graphene oxide/reduced graphene oxide and their nanocomposites, Nano Mater. Sci. 1 (2019) 31–47.

[47] A.K. Geim, Graphene prehistory, Phys. Scr. 2012 (2012) 014003.

[48] J. Chen, B. Yao, C. Li, G. Shi, An improved Hummers method for eco-friendly synthesis of graphene oxide, Carbon N. Y. 64 (2013) 225–229.

[49] D.R. Dreyer, S. Park, C.W. Bielawski, R.S. Ruoff, The chemistry of graphene oxide, Chem. Soc. Rev. 39 (2010) 228–240.

[50] Y. Xiang, L. Xin, J. Hu, C. Li, J. Qi, Y. Hou, X. Wei, Advances in the applications of graphene-based nanocomposites in clean energy materials, Crystals. 11 (2021) 1–26.

[51] P.S. Zade, M.B. Mandake, S. Walke, N. Mumbai, Review: Epoxidation of Vegetable oils, 5 (2018) 542–548.

[52] M. Desroches, M. Escouvois, R. Auvergne, S. Caillol, B. Boutevin, From vegetable oils to polyurethanes: Synthetic routes to polyols and main industrial

products, Polym. Rev. 52 (2012) 38–79.

[53] M. Fallah-Mehrjardi, A.R. Kiasat, K. Niknam, Nucleophilic ring-opening of epoxides: trends in β-substituted alcohols synthesis, J. Iran. Chem. Soc. 15 (2018) 2033–2081.

[54] J. Hong, Q. Luo, B.K. Shah, Catalyst- and solvent-free “click” chemistry: A facile approach to obtain cross-linked biopolymers from soybean oil, Biomacromolecules. 11 (2010) 2960–2965.

[55] X. Kong, G. Liu, H. Qi, J.M. Curtis, Preparation and characterization of high-solid polyurethane coating systems based on vegetable oil derived polyols, Prog. Org. Coatings. 76 (2013) 1151–1160.

[56] S. Dworakowska, A. Cornille, D. Bogdal, B. Boutevin, S. Caillol, Thiol-Ene Coupling of High Oleic Sunflower Oil towards Application in the Modification of Flexible Polyurethane Foams, Materials (Basel). 15 (2022) 628.

[57] D. Abril-Milán, O. Valdés, Y. Mirabal-Gallardo, A.F. de la Torre, C. Bustamante, J. Contreras, Preparation of renewable bio-polyols from two species of Colliguaja for Rigid polyurethane foams, Materials (Basel). 11 (2018) 2244.

[58] Q. Wang, Y. Wang, Q. Meng, T. Wang, W. Guo, G. Wu, L. You, Preparation of high antistatic HDPE/polyaniline encapsulated graphene nanoplatelet composites by solution blending, RSC Adv. 7 (2017) 2796–2803.

[59] J. Kusuma, R.G. Balakrishna, S. Patil, M.S. Jyothi, H.R. Chandan, R. Shwetharani, Exploration of graphene oxide nanoribbons as excellent electron conducting network for third generation solar cells, Sol. Energy Mater. Sol. Cells. 183 (2018) 211–219.

[60] Y. seok Jun, S. Habibpour, M. Hamidinejad, M.G. Park, W. Ahn, A. Yu, C.B. Park, Enhanced electrical and mechanical properties of graphene nano-ribbon/thermoplastic polyurethane composites, Carbon. 174 (2021) 305–316.

[61] F.W. Low, C.W. Lai, S.B. Abd Hamid, Surface modification of reduced graphene oxide film by Ti ion implantation technique for high dye-sensitized solar cells performance, Ceram. Int. 43 (2017) 625–633.

[62] N.M.S. Hidayah, W.W. Liu, C.W. Lai, N.Z. Noriman, C.S. Khe, U. Hashim, H.C. Lee, Comparison on graphite, graphene oxide and reduced graphene oxide: Synthesis and characterization, AIP Conf. Proc. 1892 (2017) 150002.

[63] B.N. Jang, D. Wang, C.A. Wilkie, Relationship between the solubility parameter of polymers and the clay dispersion in polymer/clay nanocomposites and the role of the surfactant, Macromolecules. 38 (2005) 6533–6543.

[64] S.K. Yadav, J.W. Cho, Functionalized graphene nanoplatelets for enhanced mechanical and thermal properties of polyurethane nanocomposites, Appl. Surf. Sci. 266 (2013) 360–367.

[65] T. Kuila, S. Bose, C.E. Hong, M.E. Uddin, P. Khanra, N.H. Kim, J.H. Lee, Preparation of functionalized graphene/linear low density polyethylene composites by a solution mixing method, Carbon 49 (2011) 1033–1037.

[66] M. Strankowski, P. Korzeniewski, J. Strankowska, A.S. Anu, S. Thomas, Morphology, mechanical and thermal properties of thermoplastic polyurethane containing reduced graphene oxide and graphene nanoplatelets, Materials (Basel). 11 (2018) 19.

[67] C. Xiang, P.J. Cox, A. Kukovecz, B. Genorio, D.P. Hashim, Z. Yan, Z. Peng, C.C.

Hwang, G. Ruan, E.L.G. Samuel, P.M. Sudeep, Z. Konya, R. Vajtai, P.M. Ajayan, J.M. Tour, Functionalized low defect graphene nanoribbons and polyurethane composite film for improved gas barrier and mechanical performances, ACS Nano. 7 (2013) 10380–10386.

[68] J. Zhang, C. Zhang, S.A. Madbouly, In situ polymerization of bio-based thermosetting polyurethane/graphene oxide nanocomposites, J. Appl. Polym. Sci. 132 (2015) 1–8.

[69] P. Pokharel, D.S. Lee, Thermal and mechanical properties of reduced graphene oxide/polyurethane nanocomposite, J. Nanosci. Nanotechnol. 14 (2014) 5718–5721.

[70] M.R. Zakaria, M.H. Abdul Kudus, H. Md. Akil, M.Z. Mohd Thirmizir, Comparative study of graphene nanoparticle and multiwall carbon nanotube filled epoxy nanocomposites based on mechanical, thermal and dielectric properties, Compos. Part B Eng. 119 (2017) 57–66.

[71] R. Nadiv, M. Shtein, M. Buzaglo, S. Peretz-Damari, A. Kovalchuk, T. Wang, J.M. Tour, O. Regev, Graphene nanoribbon-Polymer composites: The critical role of edge functionalization, Carbon 99 (2016) 444–450.

[72] A. Navidfar, L. Trabzon, Graphene type dependence of carbon nanotubes/graphene nanoplatelets polyurethane hybrid nanocomposites: Micromechanical modeling and mechanical properties, Compos. Part B Eng. 176 (2019) 107337.

[73] T.K. Gupta, B.P. Singh, R.K. Tripathi, S.R. Dhakate, V.N. Singh, O.S. Panwar, R.B. Mathur, Superior nano-mechanical properties of reduced graphene oxide

reinforced polyurethane composites, RSC Adv. 5 (2015) 16921–16930.

[74] R. Shamsi, M. Koosha, M. Mahyari, Improving the mechanical, thermal and electrical properties of polyurethane- graphene oxide nanocomposites synthesized by in-situ polymerization of ester-based polyol with hexamethylene diisocyanate, J. Polym. Res. 23 (2016) 1–11.

[75] M.R. Amri, F.M. Yasin, L.C. Abdullah, S.S.O. Al-Edrus, S.F. Mohamad, Ternary nanocomposite system composing of graphene nanoplatelet, cellulose nanofiber and jatropha oil based waterborne polyurethane: Characterizations, mechanical, thermal properties and conductivity, Polymers (Basel). 13 (2021) 1–17.

[76] A. Trajcheva, N. Politakos, B.T. Pérez, Y. Joseph, J. Blazevska Gilev, R. Tomovska, QCM nanocomposite gas sensors – Expanding the application of waterborne polymer composites based on graphene nanoribbon, Polymer (Guildf). 213 (2021) 123335.

[77] X. Liu, Y. Li, W. Guo, X. Sun, Y. Feng, D. Sun, Y. Liu, K. Yan, Z. Wu, B. Su, J. Yin, Dielectric and mechanical properties of polyimide composite films reinforced with graphene nanoribbon, Surf. Coatings Technol. 320 (2017) 497–502.

[78] Y. Yoon, H. Kye, W.S. Yang, J.W. Kang, Comparing graphene oxide and reduced graphene oxide as blending materials for polysulfone and polyvinylidene difluoride membranes, Appl. Sci. 10 (2020) 2015.

[79] K.K. Patel, R. Purohit, Ultrasonic Vibration-Induced Shape Memory Polymer (Polyurethane)/Graphene Nanoplatelets Composite, J. Inst. Eng. Ser. D. 101 (2020) 141–149.